DYNAMOMETER PROPORTIONAL LOAD CONTROL

SRUJAN KUSUMBA

Bachelor of Engineering in Electrical and Electronics Engineering

Kakatiya University, India

May, 2001

Submitted in partial fulfillment of requirements for the degree

MASTER OF SCIENCE IN ELECTRICAL ENGINEERING

at the

CLEVELAND STATE UNIVERSITY

December, 2004

To my beloved parents Dr. Seetha Rama Rao & Revathi, brother Kiran,
Babai, Pinnai, Manish, Niteesh,
Atha, Mama, Swetha &Thirumal.

ACKNOWLEDGEMENT

I would like to express my sincere indebtness and gratitude to my thesis advisor Dr. Dan Simon, for the ingenious commitment, encouragement and highly valuable advice he provided me over the entire course of this thesis.

I would also like to thank Dennis Feucht of Innovatia Labs, and Tom Priolo for providing the hardware support and technical assistance during the development of thesis project.

I would also like to thank my committee members Dr. Ana Stankovic and Dr. Majid Rashidhi for their support and advice. I should not forget to thank Dr. Eugenio Villaseca for funding me through my course of study and his academic advice.

I also like to thank my lab mates at the Embedded Control Systems Research Laboratory for their encouragement and intellectual input during the entire course of this thesis, without which this work wouldn't have been possible.

Finally, I wish to thank my parents and my roommates who have always been a constant source of inspiration to me.

DYNAMOMETER PROPORTIONAL LOAD CONTROL

SRUJAN KUSUMBA

ABSTRACT

Dynamometers are electro-mechanical instruments used to place a controlled mechanical load on torque-producing devices such as motors. They are used to characterize motor torque as a function of speed. A dyno is a controlled, mechanical, rotational load. It controls either speed or torque and measures both. With a dyno, the torque-speed curves of motors can be plotted, and their motor-drives can be tested over the intended operating range. Dynos are to motors and motor drives as oscilloscopes are to electronics – a basic test instrument.

A typical bench-top dyno costs $10,000 or more. The corresponding electronics test instrument, the digital storage oscilloscope, can be bought for around $1,000, a rather sizeable difference. Consequently, for small laboratories on limited budgets, it can make sense to build a dynamometer for testing the motors. The goal of this thesis is to build a cost efficient dynamometer for small motor performance testing.

Speed control is done using an H-bridge configuration of the MOSFETs to PWM the load current through R_{load} (load resistance). The speed at which the motor is running is measured by using an optical encoder attached on the shaft of the generator and the reference speed is set by the user by using a potentiometer. The error speed then is sent to the controller which changes the duty cycle of the PWM (switching of the MOSFETs) to change the load current.

CONTENTS

LIST OF FIGURES x

LIST OF TABLES xii

CHAPTER I -- INTRODUCTION 1

1.1 DYNAMOMETER SYSTEM 2

1.2 MOTIVATION 3

1.3 THESIS ORGANIZATION 4

CHAPTER II -- DYNAMOMETERS 6

2.1 INTRODUCTION 6

2.1.1 Motivation 7

2.1.2 Dynamometer Applications 9

2.2 TYPES OF DYNAMOMETERS 9

2.2.1Hysteresis Dynamometers 9

2.2.1.1 The Hysteresis Braking System 10

2.2.1.2 Advantages of Hysteresis Devices 12

2.2.1.3 Other Types of Hysteresis Dynamometers 13

2.2.2 Eddy Current Dynamometers 14

2.2.3 Powder Brake Dynamometers 16

2.2.4 Baby Dynamometers 17

CHAPTER III – PERMANENT MAGNET DC MOTORS 21

3.1 INTRODUCTION 21

3.2 CONSTRUCTION 22

3.3 PERFORMANCE 24

3.4 ADVANTAGES AND DISADVANTAGES 26

3.4.1 Advantages 26

3.4.2 Disadvantages 27

3.5 MOTOR EQUATIONS 28

3.5.1 Internal Generated Voltage 28

3.5.2 Induced Torque 30

3.6 DYNAMOMETER PMDC MOTORS SPECIFICATIONS AND CALCULATIONS 32

CHAPTER IV—MOTOR CONTROL DEVELOPMENT BOARD 35

4.1 INTRODUCTION 36

4.2 SYSTEM SPECIFICATIONS 38

4.2.1 Processor 38

4.2.1.1 High Performance Modified RISC CPU 39

4.2.1.2 DSP Engine Features 40

4.2.1.3 Peripheral Features 40

4.2.1.4 Motor Control PWM Module Features 41

4.2.1.5 Quadrature Encoder Interface Module Features 42

4.2.1.6 Analog Features 44

4.2.1.7 Special Microcontroller Features *46*

4.2.2Power Supply *46*

4.2.3Incircuit Debugging and ICSP *47*

4.2.4Motor Position Feedback Interface *48*

4.2.5Oscillator *49*

4.2.6 RS-232 Serial Port *49*

4.2.7 RS-485 Serial Bus *49*

4.2.8 CAN Bus *50*

4.2.9 LCD Display *50*

4.2.10 LED's *51*

4.2.11 Push Button Switches *51*

4.2.12Potentiometers *52*

4.2.13Prototyping Area *52*

CHAPTER V – DC MOTOR MODELING AND PID CONTROL 53

5.1 INTRODUCTION 53

5.2 ARMATURE OR RHEOSTATIC CONTROL METHOD 54

5.3 PMDC MOTOR/GENERATOR MATHEMATICAL MODELING 56

5.3.1 Modeling *56*

5.3.2 Simulations *61*

5.4 PMDC MOTOR GENERATOR SET MATHEMATICAL MODELING 63

5.4.1 Modeling *63*

5.4.2 Simulations for Dyno Model *66*

5.5 PROPORTIONAL INTEGRAL DERIVATIVE CONTROL 69

5.5.1 Introduction..... 69

5.5.2PID Controller..... 70

5.5.3 PID Characteristics 71

5.5.4 Simulations for the Dyno System using PID Controller 72

5.6 EXPERIMENTAL RESULTS 75

CHAPTER VI – CONCLUSIONS AND FUTURE WORK 80

6.1 CONCLUSIONS 80

6.2 FUTURE WORK 81

REFERENCES 82

LIST OF FIGURES

FIGURE ..... PAGE

2.1 Hysteresis braking system 11

2.2 Water circulation system 15

2.3 Inside view of powder dynamometer 16

2.4 Block diagram of baby dynamometer system 19

2.5 Dynamometer system used for the project 20

3.1 PMDC motor construction 23

3.2 PMDC motor performance curves 25

3.3 PMDC motor performance curves varying with voltage 25

3.4 PMDC motors used in the dynamometer project 32

4.1 MC1 motor control development board 37

4.2 dsPIC30F6010 pin diagram 38

4.3 PWM module block diagram 41

4.4 Quadrature encoder interface signals 43

4.5 10 bit A/D block diagram 45

5.1 (a) Armature resistance control 54

5.1 (b) Speed/armature current characteristics 54

5.2 Schematic representation of PMDC machine 56

5.3 Schematic diagram of permanent-magnet electrical machine (current direction corresponds to motor operation) 57

5.4 Simulink block diagram of a permanent-magnet DC motor 58

5.5 Torque speed characteristic curves for permanent magnet motors 59

5.6 Torque speed and load characteristic curves for dyno motor 60

5.7 Simulink model to simulate the dyno motor 62

5.8 Motor angular velocity waveform 63

5.9 Schematic diagram of permanent magnet DC generator driven by DC motor (MUT) 64

5.10 Simulink diagram to simulate the motor-generator dynamics 67

5.11 Plot of angular speeds (ω) for different loads (R_L) 68

5.12 Plot of steady state angular speeds (ω) for different loads (R_L) 69

5.13 Unity feedback system 70

5.14 Speed plot with a P controller for a reference speed of 80 rad/sec 73

5.15 Speed plot with a PD controller for a reference speed of 80 rad/sec 74

5.16 Speed plot with a PID controller for a reference speed of 80 rad/sec 75

5.17 Tachometer and PWM signals for reference speed of 1023 rpm 76

5.18 Watch window for reference speed of 1023 rpm 76

5.19 Tachometer and PWM signals for reference speed of 765 rpm 77

5.20 Watch window for reference speed of 765 rpm 78

5.21 Tachometer and PWM signals for reference of speed of 434 rpm 78

5.22 Watch window for reference speed of 434 rpm 79

LIST OF TABLES

TABLE ..... PAGE

I. PID Characteristics …….....72

CHAPTER I

INTRODUCTION

The dynamometer system is intended to be used as a test instrument to test the speed and torque capabilities of a motor and controller combination. Dynamometers are electro-mechanical instruments used to place a controlled mechanical load on torque-producing devices such as motors. They can be used to characterize motor torque as a function of speed. A dynamometer (dyno) is a basic electro-mechanical instrument used in the development of motors and motor drives. A dyno is a controlled, mechanical, rotational load. It controls either speed or torque and measures both. With a dyno, the torque-speed curves of motor can be plotted, and their motor drives can be tested over the intended operating range. Dynos are to motors and motor drives as oscilloscopes are to electronics – a basic test instrument [1].

A typical bench-top dyno costs $10,000 or more. The corresponding electronics test instrument, the digital storage oscilloscope, can be bought for around $1,000, a rather sizeable difference. Consequently, for small laboratories on limited budgets, it can make

sense to build a dynamometer for testing the motors. This thesis project goal is to build a cost efficient dynamometer for small motor testing [2].

1.1 Dynamometer System

The dynamometer that has been developed in this thesis will be discussed in this section. The dynamometer system has two major component assemblies. The first is a 1.25 HP DC motor fastened to an MUT (motor under test) shaft. The second major component assembly is the dynamometer controller cabinet. A single board motor control development (dsPIC30F6010) is the microcontroller used to control the motor. Developing C code using a C-compiler for the controller and hardware assembly is done as part of the thesis.

Usually, the test operator will fasten his MUT to the dyno test plate and use a shaft coupling to tie the MUT shaft to the load module or generator. The two motor shafts must be exactly on the same axis. On the dyno controller, the operator sets the counter-torque that he wants to force against his motor. The dyno has a tachometer takeoff point and a tachometer read-out on a visual display. The operator can see if his controller and motor combination are strong enough to keep the motor spinning at the assigned speed against the dyno counter-torque. The operator can also set the speed or torque to which the MUT can be driven to, and test the motor speed torque capabilities.

The dyno counter-torque can be steadily increased to find the point at which the MUT can no longer spin against the counter-torque. Readings of the MUT winding current can be made under these conditions to see the operational limits of its controller.

The speed and torque control are done using an H-Bridge configuration of the FET's to PWM the load current through the load resistance R_{load}. The PWM signal is obtained from the controller cabinet (dsPIC30F6010).

1.2 Motivation

This baby dynamometer development was started about seven years ago by Dennis Feucht and Jim Skinner [2]. For several years the equipment was not used and the dyno was unfinished. Before this thesis project, Tom Priolo worked on it for his senior design project [1] but he could not implement an automatic controller. When this thesis was begun, most of the hardware circuitry was not working and a fundamental change in the theory of operation was made. The servo amplifier was not working so the theory of operation for speed control of the DC motor was changed to varying load current by a PWM method. There are no specific books or material on dynamometers but Tom Priolo's report was helpful for understanding the dyno. Some literature search on websites such as Magtrol, a dyno manufacturer, was also helpful in understanding the dyno and its working. The microcontroller that was originally designed into the dyno controller was obsolete by the time this thesis was begun, and was programmed in Forth and 6502 assembly language. At the beginning of this thesis work the microcontroller was changed to use the MC1 motor control development board from Microchip, which involved more changes to the dyno hardware.

Initial literature search on dynamometers provided a quick start on the thesis, and also the manual for Magtrol's [3] DSP6000 programmable dynamometer controller was helpful in understanding how to build a controller for a dyno. The Embedded Control

Systems Research Lab at CSU has a Magtrol hysteresis brake dynamometer, and the baby dynamometer was built along the same lines. There are some functions which are not considered in the design of the baby dynamometer due to its limitations.

1.3 Thesis organization

The current thesis makes an attempt to build a low cost, energy efficient dynamometer. Dynamometers for low cost applications are not readily available on the market and if they are available they are expensive compared to other test equipment. Instead of using hysteresis braking which dissipates the energy as heat, in this thesis a generator was used as a brake. The generated DC voltage can be converted to AC which can be controlled and can be supplied to the main power supply thus providing energy savings.

Chapter II introduces dynamometers, their applications, and their various types. The chapter also discuses various types of dynamometer braking. The chapter supports the explanation with suitable figures describing the hardware. The applications, and the advantages and disadvantages of different types of dynamometers are explained in separate sections. The last section of Chapter II describes the kind of dynamometer built for this thesis, along with its theory of operation.

Chapter III describes the construction, operation, performance, and equations governing the PMDC motor used in the dyno. Torque-speed characteristics of the motor are shown. The specifications of the PMDC motors that have been used for the thesis are mentioned and used in motor performance calculations. Section 3.2 discusses the construction of the PMDC motors and the type of materials used for the permanent

magnets. Section 3.3 deals with the performance of PMDC motors and discusses their torque-speed curves. Section 3.4 describes some of the advantages and disadvantages of PMDC motors. Section 3.5 discusses the operation of a PMDC motor and develops the model equations. Section 3.6 gives the name plate details for both of the motors used in this thesis. Some calculations are shown for use in the simulations of the motor and generator, which are presented in Chapter V.

Chapter IV discusses the second major component of the dynamometer system – the motor control development board. Section 4.1 introduces the development board and its components with Figure 4.1 showing the hardware circuitry. Section 4.2 discusses the MC1 development board specifications and provides detailed data on all the components used in this thesis. The processor that is used is a Microchip dsPIC30F6010, with capabilities such as QEI, motor control PWM, LCD display, and A/D conversion.

Chapter V presents the control method adopted in the thesis. Chapter V also has the simulation results after the motor and dynamometer modeling is described. Different control algorithms along with the simulation results are clearly shown towards the end of the chapter. At the end of the chapter experimental results obtained with the controller applied are discussed.

CHAPTER II

DYNAMOMETERS

2.1 Introduction

The dynamometer system is intended to be used as a test instrument to test the speed and torque capabilities of a motor and controller combination. Dynamometers are electro-mechanical instruments used to place a controlled mechanical load on torque-producing devices such as motors. They are used to characterize motor torque as a function of speed. A *dynamometer* (dyno) is a basic electro-mechanical instrument used in the development of motors and motor drives. A dyno is a controlled, mechanical, rotational load. It controls either speed or torque and measures both. With a dyno, the torque-speed curves of motors can be plotted, and their motor-drives can be tested over the intended operating range. Dynos are to motors and motor drives as oscilloscopes are to electronics – a basic test instrument [1].

Rotational speed is usually measured with a shaft encoder, and torque with a torque sensor. The load is usually a brake or a generator. A brake is an active electromechanical device. Its resistance to rotation is controlled by a small field current.

For smaller dynos, total mechanical power loss in the load can be tolerable. These hysteresis brakes are found on dynos of leading suppliers, such as Magtrol and Vibrac.

2.1.1 Motivation

Bench-top dynamometers (dynos) are a specialized kind of instrument and are typically costly due to limited market demand. Consequently, motor designers or users who have a limited budget may not be able to afford the $10,000 commercial units, and may not be able to find a less costly unit in the used or surplus markets. The remaining alternative is to build a dyno from low-cost components. Instead of using a hysteresis brake for the motor load, we are using a 1 KW brush motor interfaced to a commercial motor-drive with regenerative braking. The drive input will be a microcomputer that will close either a commanded speed or torque loop and also drive the front-panel [2].

A typical bench-top dyno costs $10,000 or more. The corresponding electronics test instrument, the digital storage oscilloscope, can be bought for around $1,000, a rather sizeable difference. Consequently, for small laboratories on limited budgets, it can make sense to build a dyno.

A more elegant approach than a brake is to regenerate, not dissipate, load power using a generator. Generated electric power can be inverted and fed back into the power line, completing the circuit of power back to the motor-drive under test. The only losses are conversion losses in the test set-up. More simply, though less efficiently, it can be dissipated in a resistor bank.

Motors are also generators. Brush motors are being replaced with Permanent Magnet Stepper (PMS) motors and are relatively low-cost on the surplus market. PMS

motors can also be used. Not only can the motor (used as a generator) provide loading, when calibrated, its output current can be a measure of load torque. This eliminates having to buy an expensive torque sensor. In low power motor testing applications one can design a dynamometer without expensive braking schemes such as hysteresis or eddy Current braking schemes. This thesis work hence emphasizes the construction of low power (less than 1 KW) motor testing equipment.

The dynamometer system that has been developed for this thesis has two major component assemblies. The first is a 1.25 HP DC motor fastened to a motor under test (MUT) shaft. The second major component assembly is the dynamometer controller cabinet. A single motor control development (microchips DSP processor, dsPIC30F6010) board is the microcontroller used to control the motor. Developing C code using a C-compiler for the controller and hardware assembly is done as part of the thesis.

Usually, the test operator will fasten his MUT to the dyno test plate and use a shaft coupling to tie the MUT shaft to the load module or generator. The two motor shafts must be exactly on the same axis. On the dyno controller, the operator sets the counter-torque that he wants to force against his motor. The dyno has a tachometer takeoff point and a tachometer read-out on the LCD. The operator can see if his controller and motor combination are strong enough to keep the motor spinning at the assigned speed against the dyno counter-torque. The operator can also set the speed or torque to which the MUT can be driven to and test the motor speed torque capabilities.

The dyno counter-torque can be steadily increased to find the point at which the MUT can no longer spin against the counter-torque. Readings of MUT winding current can be made under these conditions to see the operational limits of its controller.

2.1.2 Dynamometer Applications

Some of the applications of a dynamometer are:

1. A dyno can be used to simulate the operating conditions of a motor application.
2. The motor's response to torque loading or speed change commands under load can be studied and recorded.
3. A motor's suitability for a particular application can be determined.
4. Dynos can be used in motor repair or rewind shops to test for the effectiveness of repair.
5. Motor control research
6. Production line testing.

2.2 Types of dynamometers

Depending on the brakes or type of control used dynamometers are classified into four types. Each type of dynamometer has advantages and limitations and choosing the correct one will depend largely on the type of testing to be performed. They are:

1. Hysteresis Dynamometers (HD).
2. Eddy-Current Dynamometers (WB).
3. Powder Brake Dynamometers (PB).
4. Baby Dynamometers.

2.2.1 Hysteresis dynamometers (HD)

Hysteresis dynamometers get their name from the type of braking system that is used – hysteresis braking. Hysteresis braking system provides precise torque loading

independent of shaft speed. Hysteresis brake dynamometers (HD series) are versatile and ideal for testing in the low to middle power range (max. 14 KW intermittent duty). Hysteresis brakes do not require speed to create torque, and therefore can provide a full motor ramp from free-run to locked rotor. Brake cooling is provided by convection (no external source) or by air (compressed air or dedicated blower) depending on the model. Hysteresis dynamometers have both continuous and intermittent power ratings where the dynamometer is capable of dissipating more power for shorter periods of time. All hysteresis dynamometers have accuracy ratings of ±0.25% to ±0.5% full scale, depending on size and system configuration. Also available are special designs for high-speed motor testing [4].

2.2.1.1 The hysteresis braking system

Overview**:** The hysteresis effect in magnetism is applied to torque control by the use of two basic components –a reticulated pole structure and a specialty steel rotor/shaft assembly–fastened together but not in physical contact. Until the field coil is energized, the drag cup can spin freely on the ball bearings. When a magnetizing force from either a field coil or magnet is applied to the pole structure, the air gap becomes a flux field. The rotor is magnetically restrained, providing a braking action between the pole structure and rotor. Because torque is produced strictly through a magnetic air gap, without the use of friction or shear forces, hysteresis brakes provide absolutely smooth, infinitely controllable torque loads, independent of speed, and they operate quietly without any physical contact of interactive members [5]. As a result, with the exception of shaft bearings, no wear components exist. Hysteresis braking system can be seen in Figure 2.1

Control: In an electrically operated hysteresis brake, adjustment and control of torque is provided by a field coil. This allows for complete control of torque by adjusting dc current to the field coil. Adjustability from a minimum value to a maximum value of rated torque is possible. Additional torque in the range of 15-25% above rated torque may be available on some brakes.

The amount of braking torque transmitted by the brake is proportional to the amount of current flowing through the field coil. The direction of current flow (polarity) is of no consequence to the operation of the brake. For optimum torque stability, a dc supply with current regulation is recommended. This will help to minimize torque drift attributable to changes in coil temperature and in-line voltage, which can result in changes in coil current, and consequently, in torque.

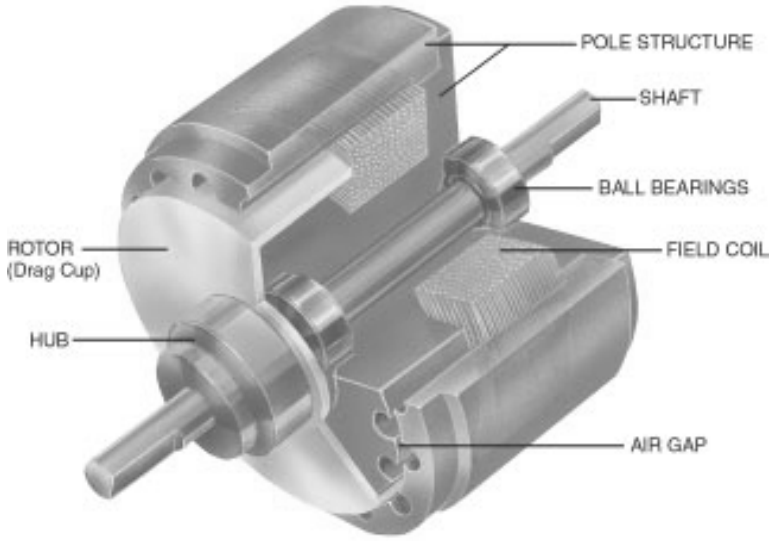

Figure 2.1: Hysteresis braking system [5]

2.2.1.2 Advantages of hysteresis devices

1) Long, maintenance-free life: Hysteresis brakes produce torque strictly through a magnetic air gap, making them distinctly different from mechanical-friction and magnetic particle devices. Because hysteresis devices do not depend on friction or shear forces to produce torque, they do not suffer the problems of wear, particle aging, and seal leakage. As a result, hysteresis devices typically have life expectancies many times that of friction and magnetic particle devices.

2) Life cycle cost advantages: While the initial cost of hysteresis devices may be the same or slightly more than that of their counterparts, the high cost of replacing, repairing and maintaining friction and magnetic particle devices often makes hysteresis devices the most cost-effective means of tension and torque control available.

3) Operational smoothness: Because they do not depend on mechanical friction or particles in shear, Hysteresis brakes are absolutely smooth at any slip ratio. This feature is often critical in wire drawing, packaging and many other converting applications.

4) Superior torque repeatability: Because torque is generated magnetically without any contacting parts or particles, Hysteresis brakes provide superior torque repeatability. Friction and magnetic particle devices are usually subject to wear and aging with resultant loss of repeatability. Hysteresis devices will repeat their performance precisely, to ensure the highest level of process control.

5) Broad speed range: Hysteresis devices offer the highest slip speed range of all electric torque control devices. Depending on size, kinetic power requirements and bearing loads, many hysteresis brakes can be operated at speeds in excess of 10,000 rpm.

In addition, full torque is available even at zero slip speed and torque remains absolutely smooth at any slip speed.

6) Excellent environmental stability: Hysteresis devices can withstand significant variation in temperature and other operating conditions. In addition, because they have no particles or contacting active parts, hysteresis brakes are extremely clean.

2.2.1.3 Other types of hysteresis dynamometers

2.2.1.3.1 Engine dynamometers

With an engine dynamometer, high performance motor testing is available for small gas engines. Engine dynamometers have been designed to address the severe, high vibration conditions inherent in internal combustion engine testing [6].

Engine dynamometers are part of hysteresis dynamometers so they are highly accurate (±0.25% of full scale) and can be controlled either manually or via a PC-based dynamometer controller. For a small engine test stand, engine dynamometer offers a full line of controllers, readouts and data acquisition software.

An engine dynamometer is ideally suited for emissions testing as set forth in CARB and EPA clean air regulations. The dynamometers will offer superior performance on the production line, at incoming inspection or in the R&D lab.

As with all hysteresis dynamometers, engine loading is provided by hysteresis braking, which provides: torque independent of speed, including full load at 0 rpm, excellent repeatability; frictionless torque with no wearing parts (other than bearings); and long operating life with low maintenance

2.2.1.3.2 Dial weight dynamometers

The most important characteristic of any measurement instrument is repeatability and accuracy. The dial weight dynamometer uses the combination of a hysteresis brake and gravity to insure constant, reliable results. The brake torque rise is directly proportional to applied current. The calibrated weight system provides readings in standard engineering units through the use of multiple torque range scales provided on each size dynamometer.

Dial weight dynamometers are a lower cost alternative to the standard (load cell) hysteresis dynamometers. The dial weight dynamometers are easy to operate, provide repeatable and accurate results, and will operate for many years with minimal maintenance. A dial weight dynamometer system can only operate manually in an open loop mode [7].

Load can be adjusted from no load to full scale through simple potentiometer control on power supply. Magnetically coupled hysteresis brake provides smooth torque application independent of shaft speed. This permits testing motors from no load to locked rotor or armature.

2.2.2 Eddy-current dynamometers (WB)

Eddy-current brake dynamometers (WB) are ideal for applications requiring high speeds and also when operating in the middle to high power range. Eddy-current brakes provide increasing torque as the speed increases, reaching peak torque at rated speed. The dynamometers have low inertia as a result of small rotor diameter. Brake cooling is provided by a water circulation system, which passes inside the stator to dissipate heat

generated by the braking power. The water cooling in the WB provides high continuous power ratings (max. 140 KW). The eddy-current brake dynamometers have accuracy ratings of ±0.3% to 0.5% full scale, depending on size and system configuration. Additional options include: high-speed version, speed pick-up, mechanical rotor blocking device and vertical mounting [8].

Regulated Cooler and Heat Exchanger: Eddy-current (WB) and powder dynamometer (PB) brakes are cooled by a water circuit. The water/air exchanger allows the energy of the closed-loop cooling circuit to dissipate. The circulation pump works permanently in order to maintain the temperature of the water in the tank. The temperature detector permanently measures and displays the temperature of the water at the output in order to regulate it.

In an effort to reduce the noise level, the regulator has two fan speeds that can be used depending on the demand for cooling. An alarm triggers if the water temperature exceeds pre-determined values. The dynamometer controller switches off the power to the dynamometer brake when it reaches the alarm threshold.

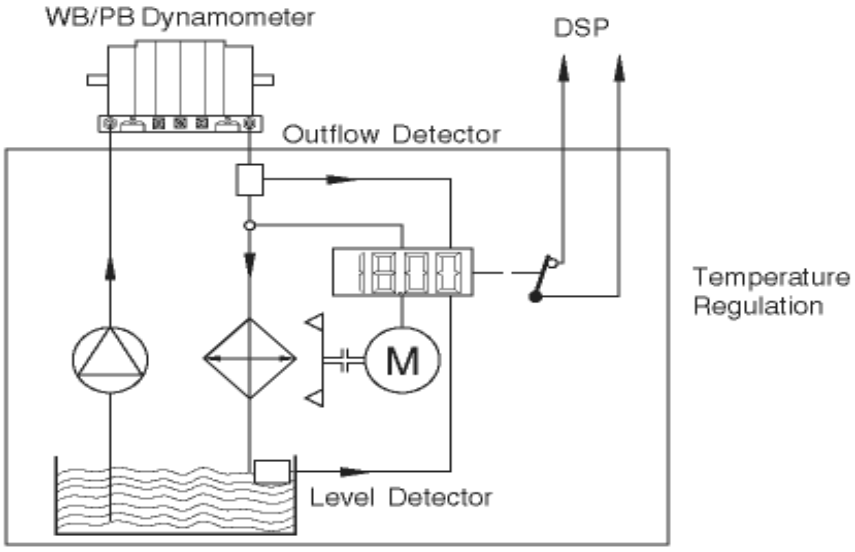

Figure 2.2: Water circulation system [9]

2.2.3 Powder brake dynamometers (PB)

The powder brake dynamometer (PB) contains, as its name suggests, a magnetic powder. The electrical current passing through the coil generates a magnetic field, which changes the property of the powder, thus producing a smooth braking torque through friction. They are ideal for applications operating in the low to middle speed range or when operating in the middle to high torque range. Like hysteresis brakes, powder brakes provide full torque at zero speed. Like the eddy-current brake dynamometers, the powder brake dynamometers are water cooled, allowing for power ratings up to 48 KW. The powder brake dynamometers have accuracy ratings of ±0.3% to 0.5% full scale, depending on size and system configuration.

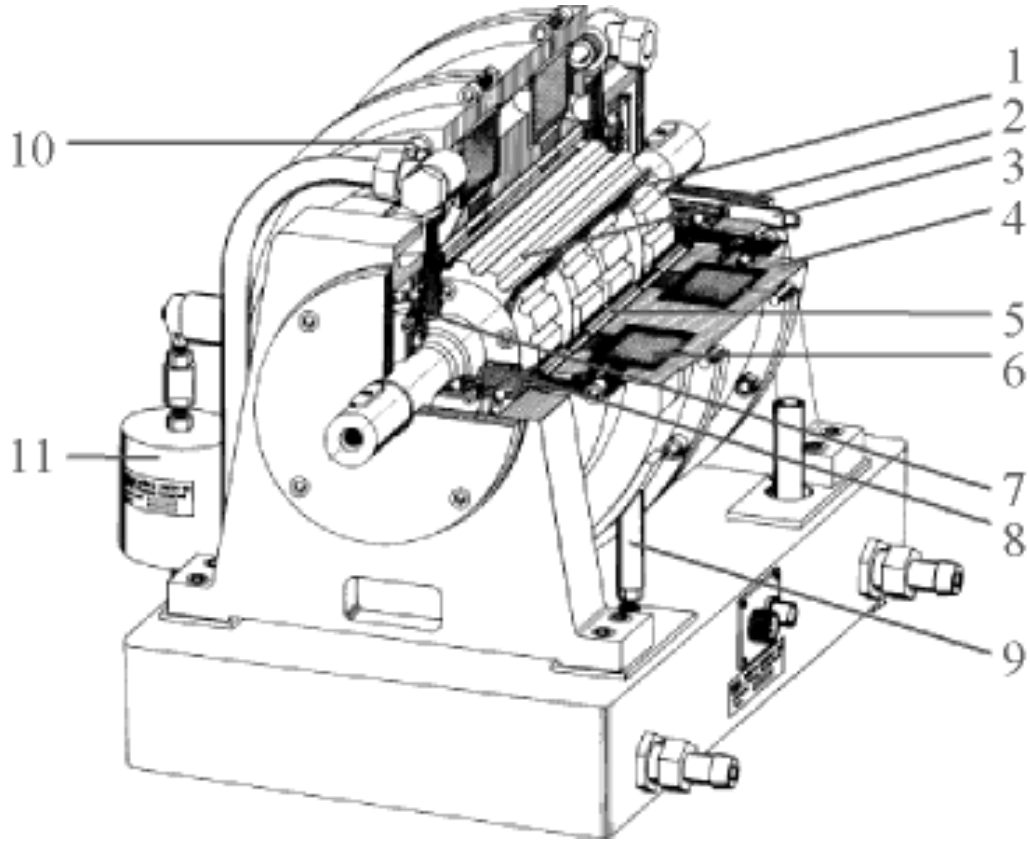

Figure 2.3: Inside view of powder dynamometer [10]

The dyno components shown in Figure 2.3 are as follows.

1. Rotor of powder dynamometer.

2. Rotor of eddy-current dynamometer.

3. Speed pickup.

4. Stator.

5. Cooling water.

6. Excitation coil.

7. Trunnion bearing.

8. Labyrinth seal.

9. Transport locking security.

10. Thermo-switch.

11. Force transducer.

2.2.4 Baby dynamometers

Baby dynamometers are used in low power braking applications where the brake doesn't dissipate lot of heat. They are ideal for applications operating in the low to middle speed range or when operating in the middle to high torque range. Motor designers or users who have a limited budget may not be able to afford the $10,000 commercial dynamometers, and may not be able to find a less costly unit in the used or surplus markets. The remaining alternative is to build a baby dyno from low-cost components. Instead of using a hysteresis brake for the motor load, we are using a 1 KW brush motor interfaced to a commercial motor-drive with regenerative braking.

A more elegant approach than a brake is to regenerate, not dissipate, load power using a generator. Generated electric power can be inverted and fed back into the power line, completing the circuit of power back to the motor-drive under test. The only losses are conversion losses in the test set-up. More simply, though less efficiently, it can be dissipated in a resistor bank. The baby dynamometer designed in this project the load power is dissipated in the load resistor bank.

The dynamometer system has two major component assemblies. The first is a 1.25 HP DC motor fastened to a motor under test (MUT) shaft. The second major component assembly is the dynamometer controller cabinet. A single motor control development (microchips DSP processor, dsPIC30F6010) board is the microcontroller used to control the motor. Developing C code using a C-compiler for the controller and hardware assembly is done as part of the project.

Usually, the test operator will fasten his MUT to the dyno test plate and use a shaft coupling to tie the MUT shaft to the load module or generator. The two motor shafts must be exactly on the same axis. On the dyno controller, the operator sets the counter-torque that he wants to force against his motor. The dyno has a tachometer takeoff point and a tachometer read-out on the LCD. The operator can see if his controller and motor combination are strong enough to keep the motor spinning at the assigned speed against the dyno counter-torque. The operator can also set the speed or torque to which the MUT can be driven to and test the motor speed torque capabilities.

The dyno counter-torque can be steadily increased to find the point at which the MUT can no longer spin against the counter-torque. Readings of MUT winding current

can be made under these conditions to see the operational limits of its controller. The dyno can also be interfaced to the computer and data can be saved or the data can be inputted from the computer. A user friendly GUI can be developed and used to control the dyno and also data can be fetch from the microcontroller.

The basic dyno scheme used in the project is shown below:

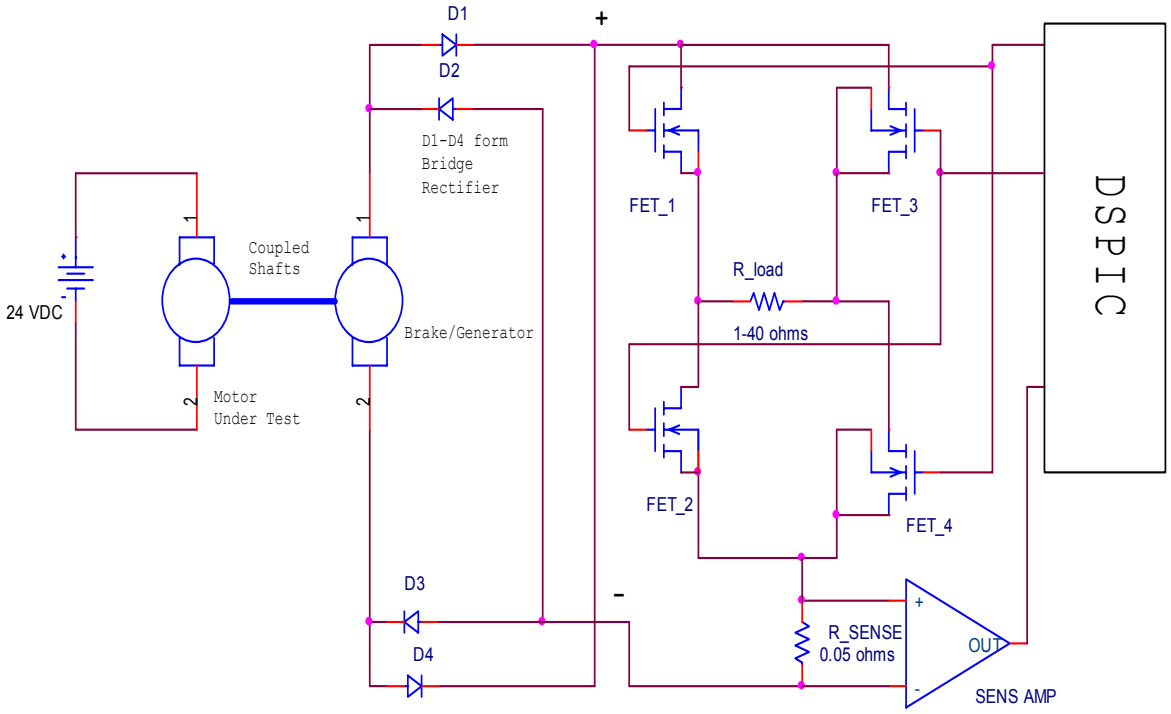

Figure 2.4: Block diagram of baby dynamometer system

The speed and torque control are done using H-bridge configuration of the FET's to PWM the load current through R_{load}. A bridge rectifier is placed between the generator and the load resistance Since no matter which way the generator rotates the FET's drain will always be connected to the positive (+) side of the generator, and the FET's source will be always connected to the negative (–) side of the generator output. Speed at which

the motor is running is measured by using an optical encoder attached on the shaft of the generator.

The optical encoder generates a pulse the frequency of the pulse is measured by the motor control development board and thus the speed. The speed measured is used for speed control by closing the loop. The current is measured using a sense resistor and thus the torque can be calculated and used for generating the PWM for the torque control.

The baby dynamometer system that has been developed for the project is shown in Figure 2.5

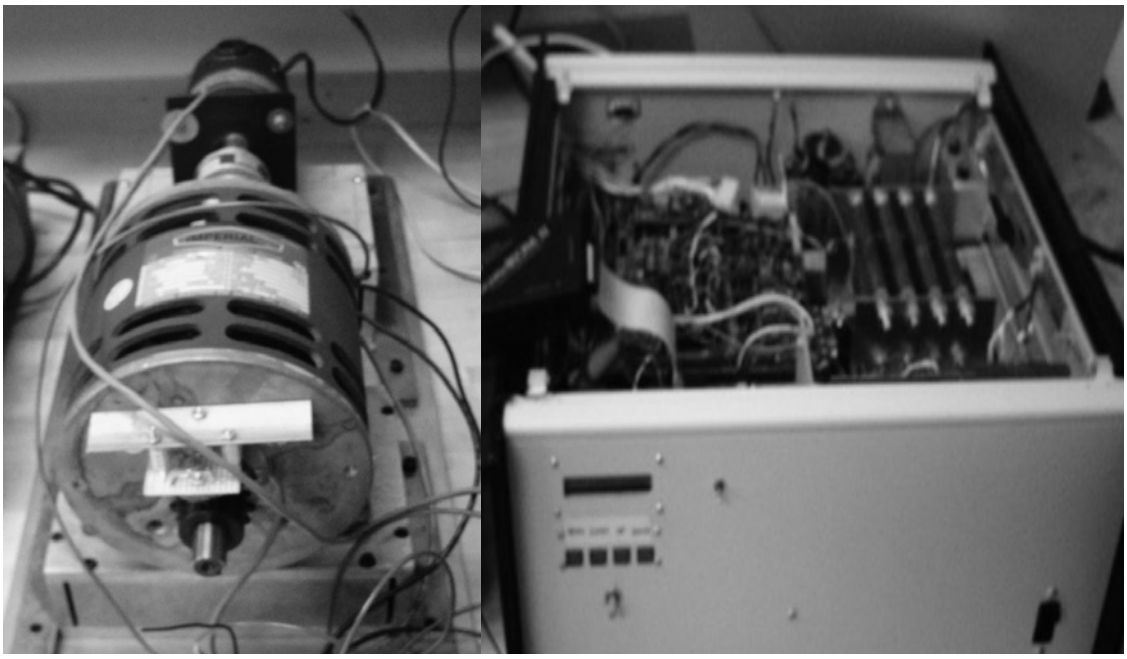

Figure 2.5: Dynamometer system used for the project

CHAPTER III

PERMANENT MAGNET DC MOTORS

3.1 Introduction

The 1.25 HP DC motor (working in generator mode) fastened to a motor under test (MUT) shaft is a permanent magnet DC motor. A permanent magnet DC (PMDC) motor is a DC motor whose poles are made of permanent magnets. This motor is used in generator mode and the current produced from it is controlled. Therefore the speed as well as the torque in the dyno system is controlled. A permanent magnet DC motor is similar to an ordinary DC shunt motor except that its field is provided by permanent magnets instead of salient pole wound field structures. The permanent magnets of the PMDC motor are supported by a cylindrical steel stator which also serves as a return path for the magnetic flux. The rotor has winding slots, commutator segments and brushes as in conventional DC machines.

This chapter describes the construction, working, performance and also equations governing the PMDC motor. Torque-speed characteristics of the motor are shown and also the specifications of the PMDC motors that have been used for the project is

mentioned and some calculations are done in the end of the chapter. Section 3.2 discusses the construction of the PMDC motors and the type of materials used for the permanent magnets. Section 3.3 deals with the performance of such a machine with the torque-speed curves. Section 3.4 describes some of the advantages and disadvantages of a PMDC motor. Next section 3.5 informs the working of a PMDC motor with the equations. Last section 3.6 has the name plate details for both the motors used in the project and also few calculations are shown, used in the simulations for the motor and generator, discussed in Chapter V.

3.2 Construction

There are three types of permanent magnets used for such motors. The materials used have residual flux density and high coercivity [11].

i. Alnico magnets – they are used in motors having ratings in the range of 1 kW to 150 kW.
ii. Ceramic (ferrite) magnets – they are economical in fractional kilowatt motors.
iii. Rare-earth magnets – made of samarium cobalt and neodymium iron cobalt which have the highest energy product. Such magnetic materials are costly but are the best economic choice for small as well as large motors.

Another form of the stator construction is the one in which permanent-magnet material is cast in continuous form of in two pieces.

Most of these motors usually run on 6V, 12V or 24V DC supply obtained either from batteries or rectified alternating current. In such motors, torque is produced by interaction

between the axial current-carrying rotor conductors and the magnetic flux produced by the permanent magnets.

Small, 12 V PMDC motors are used for driving automobile heater and air conditioner blowers, windshield wipers, windows, fans, radio antennas, etc. They are also used for electric fuel pumps, marine engine starters, wheelchairs and cordless power tools.

The toy industry uses millions of such motors which are also used in other applications such as the toothbrush, food mixer, ice crusher, portable vacuum cleaner and shoe polisher and also in portable electric tools such as drills, saber saws, hedge trimmers, etc.

The basic construction of a PMDC motor is as shown in Figure 3.1.

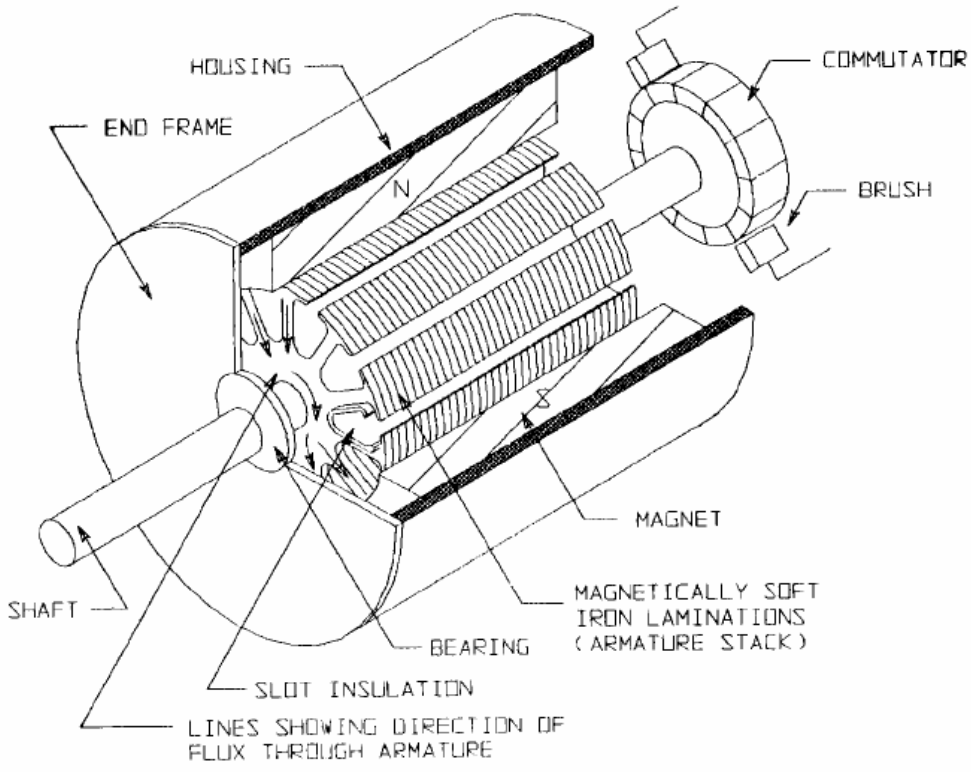

Figure 3.1: PMDC motor construction

A good material for the poles of a PMDC motor should have as large a residual flux density as possible, while simultaneously having as large a coercive magnetizing intensity as possible. The large residual flux density produces a large flux in the machine, while the large coercive magnetizing intensity means that a very large current would be required to demagnetize the poles.

In the last 40 years, a number of new magnetic materials have been developed which have desirable characteristics for making permanent magnets. The major types of materials are the ceramic (ferrite) magnetic materials and the rare-earth magnetic materials. The best rare-earth magnets produce the same residual flux as the best conventional ferromagnetic alloys, while simultaneously being largely immune to demagnetization problems due to armature reaction.

3.3 Performance

To calculate the performance for this motor, one must predict the air gap flux and calculate the no-load speed and current and the stall torque and current [12]. A straight line drawn between the no-load speed and the stall torque represents the *speed-torque curve* of the motor. A straight line drawn between the no-load current and the stall current represents the *current-torque performance curve.* The PMDC motor performance curves are shown in Figure 3.2

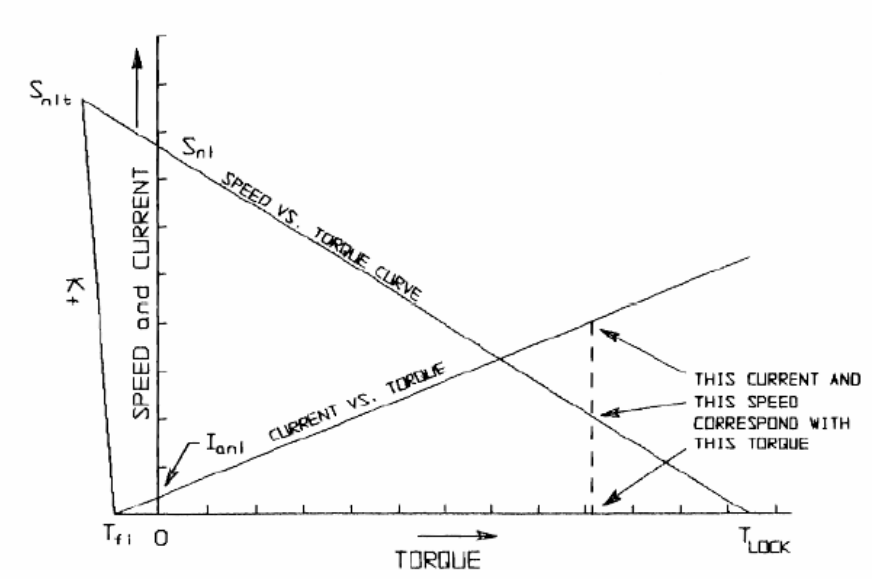

Figure 3.2: PMDC motor performance curves

The PMDC motor speed-torque curve is a straight line which makes this motor ideal for a servomotor. Moreover, input current increases linearly with load torque. The efficiency of such motors is higher as compared to wound-field DC motors because, in their case, there is no field copper loss. PMDC motor performance varying with voltage curve is shown in Figure 3.3 below

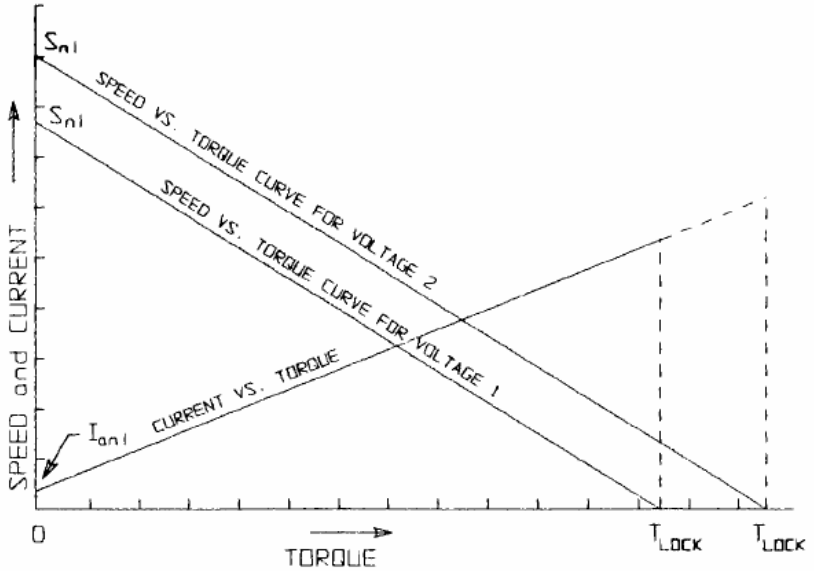

Figure 3.3: PMDC motor performance varying with voltage

As seen from the performance curves above the PMDC motor has a definite no-load speed. Hence, it doesn't 'run away' when load is suddenly thrown off, provided the field circuit remains closed. The drop in speed from no-load to full-load is small; hence this motor is usually referred to as constant speed motor. The speed for any load within the operating range of the motor can be readily obtained by varying the field current by means of a field rheostat.

It is seen from the curves that a certain value of current is required even when output is zero. The motor input under no-load conditions goes to meet the various losses occurring within the machine.

As compared to other motors, a PMDC motor is said to have a lower starting torque. But this should not be taken to mean that a shunt motor is incapable of starting a heavy load. Actually it means that series and compound motors are capable of starting heavy loads with less excess of current inputs over normal values than the PMDC motors and that consequently the depreciation on the motor will be relatively less.

3.4 Advantages and Disadvantages

3.4.1 Advantages

Permanent magnet DC motors offer a number of benefits compared with shunt dc motors in some applications. Since these motors do not require an external field circuit, they do not have the field circuit copper losses associated with shunt DC motors. PMDC motors are especially common in smaller fractional and sub fractional horsepower sizes, where the expense and space of a separate field circuit can not be justified [11].

(i) In very small ratings, use of permanent-magnet excitation results in lower manufacturing costs.

(ii) In many cases a PMDC motor is smaller in size than a wound-field DC motor of equal power rating.

(iii) Since field excitation current is not required, the efficiency of these motors is generally higher than that of the wound-field motors.

(iv) Low-voltage PMDC motors produce less air noise.

(v) When designed for low-voltage (12V or less) these motors produced very little radio and TV interference.

3.4.2 Disadvantages

PMDC motors also have disadvantages too. Permanent magnets cannot produce as high a flux density as an externally supplied shunt field, so a PMDC motor will have a lower induced torque τ_{ind} per ampere of armature current I_A than a shunt motor of the same size and construction. In addition, PMDC motors run the risk of demagnetization. The armature current I_A in a DC machine produces an armature magnetic field of it own. The armature magneto motive force (mmf) subtracts from the mmf of the poles under some portions of pole faces and adds to the mmf of the poles under other portions of the pole faces, reducing the overall net flux in the machine. This is the armature reaction effect. In a PMDC machine, the pole flux is just the residual flux in the permanent magnets. If the armature current becomes very large, there is some risk that the armature mmf may demagnetize the poles, permanently reducing and reorienting the residual flux

in them. Demagnetization may also be caused by the excessive heating which can occur during prolonged periods of overload [11].

(i) Since their magnetic field is active at all times even when motor is not being used, these motors are made totally enclosed to prevent their magnets from collecting magnetic junk from the neighborhood. Hence, as compared to wound-field motors, their temperature tends to be higher. However, it may not be much of a disadvantage in situations where motor is used for short intervals.

(ii) A more serious disadvantage is that the permanent magnets can be demagnetized by armature reaction mmf causing the motor to become inoperative. Demagnetization can result from (a) improper design (b) excessive armature current caused by a fault or transient or improper connection in the armature circuit (c) improper brush shift and (d) temperature effects.

3.5 Motor Equations

3.5.1 Internal Generated Voltage

The induced voltage in any given PMDC machine depends on three factors:

1. The flux φ in the machine.
2. The speed ω of the machine's rotor.
3. A constant depending on the construction of the machine.

The voltage out of the armature of a PMDC motor is equal to the number of conductors per current path times the voltage on each conductor. The voltage in *any single conductor under the pole faces* is known [12] to be

$$e_{ind} = e = vBl \tag{3.5.1}$$

where, ν is velocity of each conductor, B is flux density under the pole, l is length of the conductor.

The voltage out of the armature of a PMDC is:

$$E_A = \frac{Z\nu Bl}{a} \tag{3.5.2}$$

Where Z is the total number of conductors and a is the number of current paths. The velocity of each conductor (ν) in the rotor can be expressed as ν = rω, where r is the radius.

$$E_A = \frac{Zr\omega Bl}{a} \tag{3.5.3}$$

This voltage can be reexpressed in a more convenient form by noting that the flux of a pole is the equal to the flux density (B) under the pole times the pole's area (A_P):

$$\phi = BA_P$$

The rotor of the machine is shaped like a cylinder, so its area is

$$A = 2\pi rl \tag{3.5.4}$$

If there are P poles on the PMDC, then the portion of the area associated with each pole is the total area A divided by the number of poles P:

$$A_P = \frac{A}{P} = \frac{2\pi rl}{P} \tag{3.5.5}$$

The total *flux per pole* in the PMDC motor is thus

$$\phi = BA_P = \frac{B(2\pi rl)}{P} = \frac{2\pi rlB}{P} \tag{3.5.6}$$

Therefore, the internal generated voltage in the machine can be expressed as:

$$E_A = \frac{Zr\omega Bl}{a} \tag{3.5.7}$$

$$= \left(\frac{ZP}{2\pi a} \right) \left(\frac{2\pi rlB}{P} \right) \omega$$

$$\boxed{E_A = \frac{ZP}{2\pi a} \phi\omega} \tag{3.5.8}$$

Finally,

$$\boxed{E_A = K\phi\omega} \tag{3.5.9}$$

where

$$\boxed{K = \frac{ZP}{2\pi a}} \tag{3.5.10}$$

In modern industrial practice it is common to express the speed of a machine in revolutions per minute instead of radians per second. The conversion from revolutions per minute *n* to radians per second ω is

$$\omega = \frac{2\pi}{60} n \tag{3.5.11}$$

so the voltage equation with speed expressed in terms of revolutions per minute is

$$\boxed{E_A = K'\phi n} \tag{3.5.12}$$

where

$$\boxed{K' = \frac{ZP}{60a}} \tag{3.5.13}$$

3.5.2 Induced Torque

The torque induced in any PMDC motor depends on three factors:

1. The flux φ in the machine.
2. The armature (or rotor) current I_A in the machine.
3. A constant depending on the construction of the machine

The torque on the armature of a real machine is equal to the number of conductors Z times the torque on each conductor. The torque in *any single conductor under the pole faces* is known [12] to be:

$$\tau_{cond} = rI_{cond}lB \tag{3.5.14}$$

If there are *a* current paths in the machine, then the total armature current I_A is split among the *a* current paths, so the current in a single conductor is given by

$$I_{cond} = \frac{I_A}{a} \tag{3.5.15}$$

and the torque in a single conductor on the motor may be expressed as

$$\tau_{cond} = \frac{rI_A lB}{a} \tag{3.5.16}$$

Since there are Z conductors, the total induced torque in a PMDC rotor is

$$\tau_{ind} = \frac{ZrlBI_A}{a} \tag{3.5.17}$$

The flux per pole in this motor can be expressed as

$$\phi = BA_P = \frac{B(2\pi rl)}{P} = \frac{2\pi rlB}{P} \tag{3.5.18}$$

so the total induced torque can be reexpressed as

$$\tau_{ind} = \frac{ZP}{2\pi a}\phi I_A \tag{3.5.19}$$

Finally,

$$\boxed{\tau_{ind} = K\phi I_A} \tag{3.5.20}$$

where

$$\boxed{K = \frac{ZP}{2\pi a}} \tag{3.5.21}$$

Both the internal generated voltage and the induced torque equations given above are only approximations, because not all the conductors in the motor are under the pole faces at any given time and also because the surfaces of each pole do not cover the entire 1/P fraction of the rotor's surface. To achieve greater accuracy, the number of conductors under the pole faces could be used instead of the total number of conductors on the rotor.

3.6 Dynamometer PMDC Motors Specifications and Calculations

The PMDC motors that are used in the dynamometer project are shown in Figure 3.4 below.

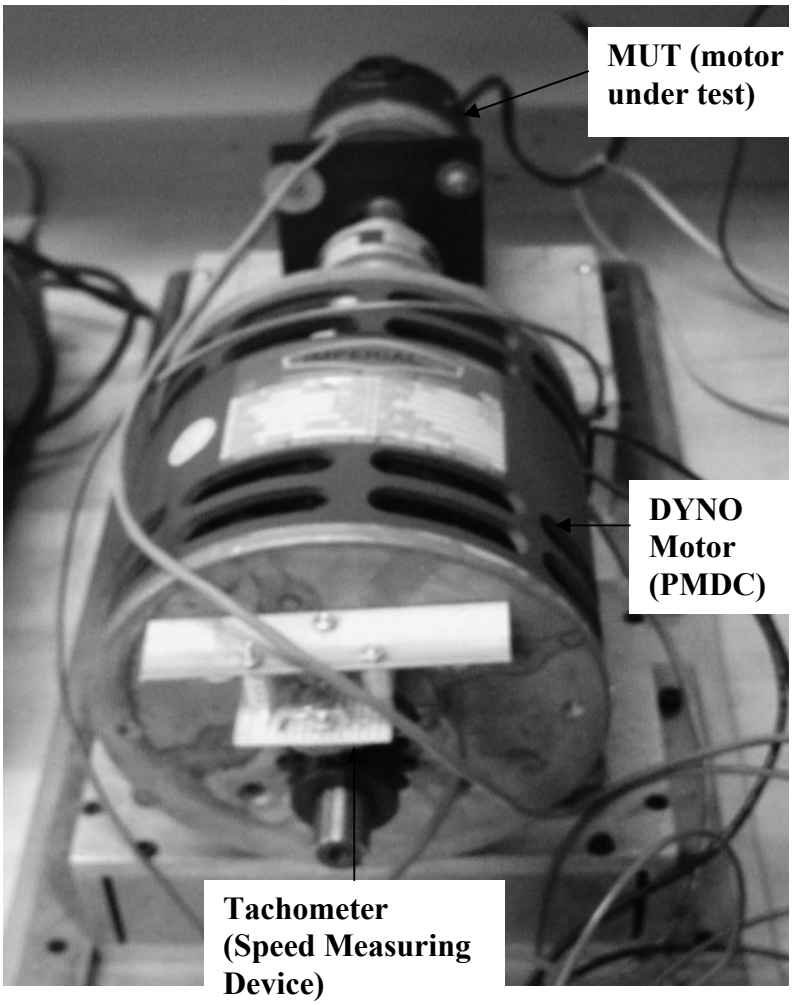

Figure 3.4 PMDC motors used in the dynamometer project

The 1.25 HP DC motor (working in generator mode) used in the baby dyno project is a brush PMDC motor and the ratings of that motor are:

Rated Voltage (V_s) = 120V DC.

Rated Current (I) = 11A.

Rated Speed (ω) = 2700rpm.

Rated Power (P) = 1.25hp.

1hp=746Watts.

1rpm = 0.1048 rad/sec

Therefore, Rated Power = 1.25hp = 1.25*746=932Watts.

Rated Speed = 2700rpm= 2700*0.1048= 283 rad/sec.

But,

$$\tau = \frac{P}{\omega} = \frac{932W}{283rad/\sec} = 330N-cm = 467oz-in \tag{3.6.1}$$

where we have used the conversion 1 N-m= 141.6 oz-in.

The torque constant (K_T) & back emf constant (K_E) can be calculated as:

$$K_T = K_E = \lambda_s = \frac{\tau}{I} = \frac{3.3N-m}{11A} = 0.30\,N-m/A = 0.30V-rad/\sec \tag{3.6.2}$$

$$V_s = v_\omega + I.R = \lambda_s.\omega + I.R = (0.3Vrad/\sec).(284\,rad/\sec) + (11A).R \tag{3.6.3}$$

$$R = \frac{35.18V}{11A} = 3.2\Omega. \tag{3.6.4}$$

$$\eta = \frac{932W}{1.32KW} = 71\% \tag{3.6.5}$$

$$\tau_0 = \lambda_s \frac{V_s}{R} = 11.25N-m \tag{3.6.6}$$

$$\omega_0 = \frac{V_s}{\lambda_s} = 400 rad / \sec = 3.82 krpm \tag{3.6.7}$$

The motor under test (MUT) shafted to the 1.25 HP motor is also a PMDC motor which is run at constant voltage of 24 V. This motor is called the prime mover since it is connected to the generator and provides the necessary torque. The model for the permanent-magnet DC generator driven by the prime mover is derived in Section 5.3. The armature resistance of the prime mover motor was measured and is r_{apm} = 3.32 Ω and the inductance of the armature is L_{apm}= 5.35 mH.

These specifications and calculations derived in this section are used in simulating the dyno system by using mathematical models derived in Section 5.3. In the earlier sections of the chapter performance and working principles have been established in brief.

CHAPTER IV

MC1 Motor Control Development Board

The second major component in the dyno system is the motor control development board. The Microchip dsPIC30F Motor Control Development Board which is fitted with a dsPIC30F6010 processor has been used in the project. The main purpose of the MC1 board is data acquisition, data processing and also display. The speed is obtained using a tachometer on the shaft of the PMDC motor which generates pulses and is read through a quadrature encoder interface (QEI) on the MC1 board. The current is also measured using sense resistors and an A/D module. The reference speed and torque are obtained from the potentiometers on the board. The speed and torque are calculated and control loops are used to process the data obtained and also calculated data is displayed on the LCD of the development board. The control loops also generate the PWM signals which are used to change the load resistance.

Section 4.1 introduces to the development board and its components with the Figure 4.1 showing the hardware circuitry. Next Section 4.2 discusses the MC1 development board specifications with detailed data on all the used components in the baby dyno project.

The processor being dsPIC30F6010 and its capabilities such as QEI, motor control PWM, LCD display, A/D module being used for the reference speed. The application of each component in the project is discussed in the respective section.

4.1 Introduction

The Microchip dsPIC30F Motor Control Development Board is used in the rapid evaluation and development of motor control applications using the motor control parts of the dsPIC family. To maximize flexibility, the largest device variant in the dsPIC family has been used. The board may be used in two different ways. First is to interface to one of the custom power modules that have been developed to complement the control board. The interface is via the 37-pin D-type connector. In this way, all the user has to supply is a motor and they are ready to go without having to worry about the power stage and signal conditioning. The power module has its own fault protection and signal isolation circuitry. There are many different feedback signals that the user can select between to customize the system to the intended application. These are selected internally within the power module. The second use of the board is for customers who already have their own power stage but are interested in evaluating the dsPIC microcontroller unit in their application. In this instance, the user can easily interface to their own system via the connectors provided on the board. Although targeted primarily at motor control applications, the board is also well suited to static power conversion applications, such as Uninterruptible Power Supplies (UPS), Power Factor Correctors (PFC) and Switch Mode Power Supplies (SMPS) [13].

All the advanced peripheral features such as LCD display, A/D modules, QEI, and PWM modules are well suited for the DYNO application hence this board is used in the project and will also help in further development of the project. Data can be transferred using this board to PC using multiple and easy methods such as RS-232 serial port, RS-485 serial bus and CAN bus. User interface can be developed on the PC for plotting the speed torque curves.

The MC1 Motor Control Development Board is shown in Figure 4.1

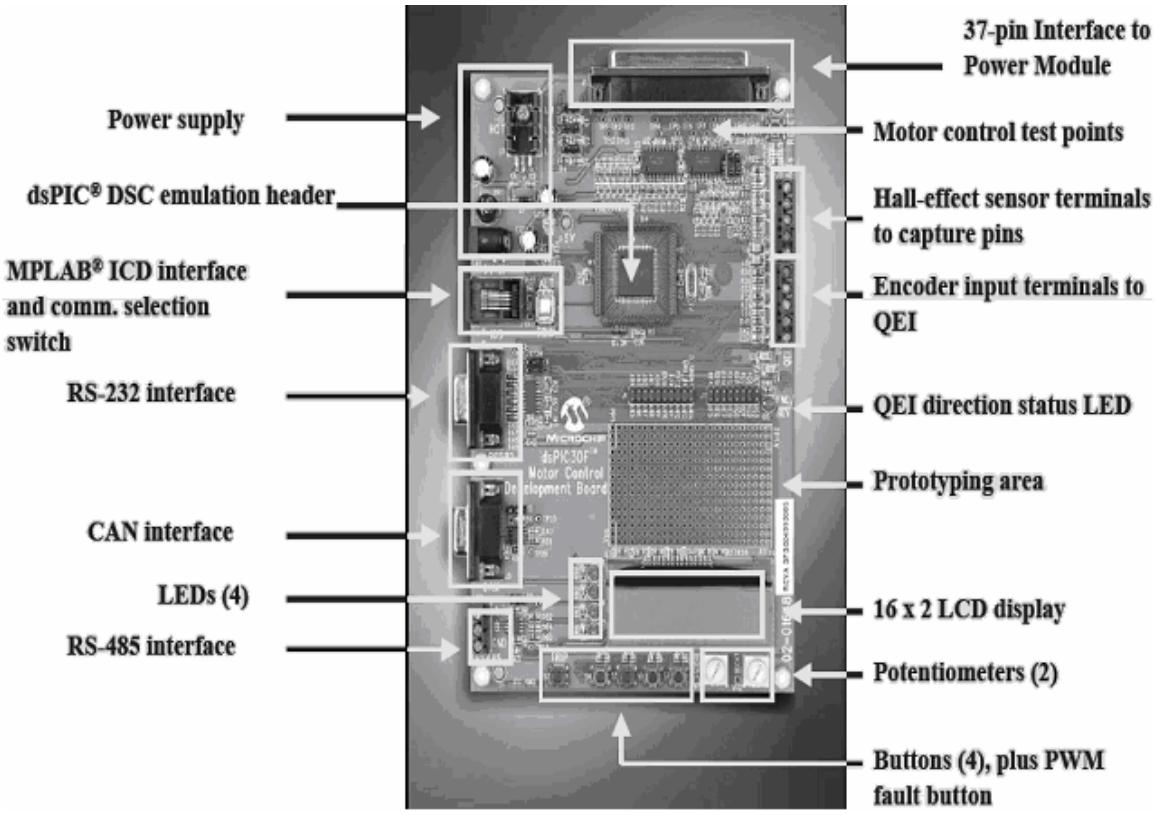

Figure 4.1: MC1 motor control development board [16]

4.2 System specifications

4.2.1 Processor

The system has the dsPIC30F6010 80-pin TQFP part fitted as the standard processor. An array of pins around the device allows the appropriate MPLAB ICE device adapter to plug directly into the board without the need for the transition socket [13]. The dsPIC30F6010 80-pin TQFP fitted on the board pin diagram is shown in Figure 4.2

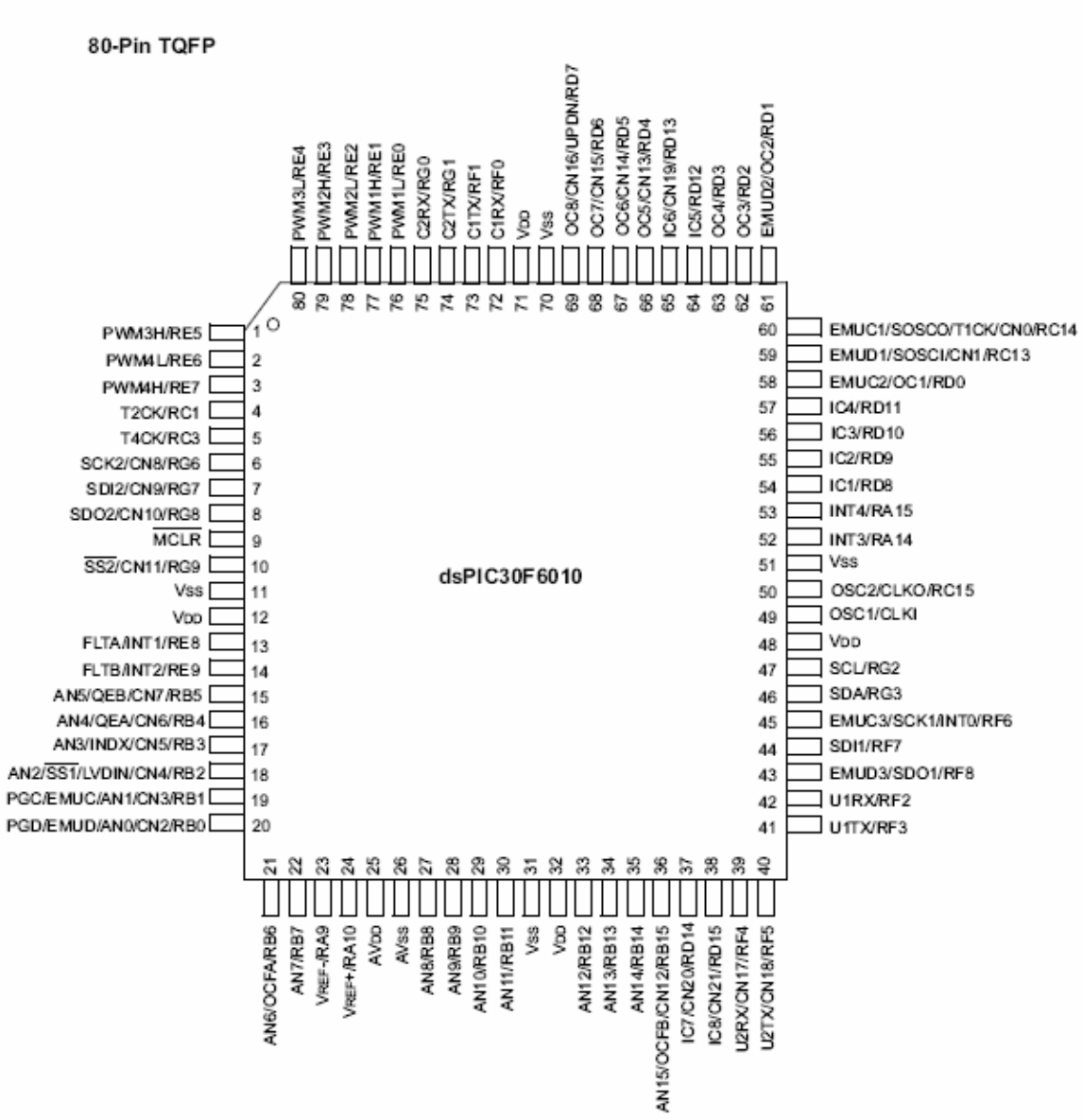

Figure 4.2: dsPIC30F6010 pin diagram [15]

The dsPIC30F devices contain extensive Digital Signal Processor (DSP) functionality within a high performance 16-bit microcontroller (MCU) architecture.

4.2.1.1 High Performance Modified RISC CPU

The dsPIC30F core is a 16-bit (data) modified Harvard architecture with an enhanced instruction set, including support for DSP. The core has a 24-bit instruction word, with a variable length opcode field. The program counter (PC) is 23-bits wide and addresses up to 4M x 24 bits of user program memory space [15].

The dsPIC30F instruction set has two classes of instructions: the MCU class of instructions and the DSP class of instructions. These two instruction classes are seamlessly integrated into the architecture and execute from a single execution unit. The instruction set includes many addressing modes and was designed for optimum C compiler efficiency. The dsPIC30F instruction set contains 84 instructions, which can be grouped into the ten functional categories. Each data word consists of 2 bytes (16 bits), and most instructions can address data either as words or bytes. The data space is 64 Kbytes (32 K words) and is split into two blocks, referred to as X and Y data memory. Each block has its own independent Address Generation Unit (AGU). Most instructions operate solely through the X memory AGU, which provides the appearance of a single unified data space.

The dsPIC30F family of devices contains 144 Kbytes of on-chip flash program space (instruction words) for executing user code. The dsPIC30F family of devices contains 4 Kbytes of non-volatile data EEPROM. The dsPIC30F6010 processor can execute up to 30 MIPS (Million Instructions Per Second). The dsPIC30F6010 has 44

interrupt sources and 4 processor exceptions (traps), which must be arbitrated based on a priority scheme. Eight user selectable priority levels for each interrupt source is another feature where the user can assign priorities for interrupts. The dsPIC30F has sixteen, 16-bit working registers. Each of the working registers can act as a data, address or offset register. The 16th working register (W15) operates as a software stack pointer for interrupts and calls.

4.2.1.2 DSP Engine Features

The DSP engine features a high speed, 17-bit by 17-bit multiplier, a 40-bit ALU, two 40-bit saturating accumulators and a 40-bit bi-directional barrel shifter. The barrel shifter is capable of shifting a 40-bit value up to 15 bits right, or up to 16 bits left, in a single cycle. The DSP instructions operate seamlessly with all other instructions and have been designed for optimal real-time performance. The MAC instruction and other associated instructions can concurrently fetch two data operands from memory while multiplying two W registers. This requires that the data space be split for these instructions and linear for all others. This is achieved in a transparent and flexible manner through dedicating certain working registers to each address space [15].

4.2.1.3 Peripheral Features

The dsPIC30F6010 device has a high current sink/source I/O pins which are 25 mA/25 mA. The dsPIC30F6010 device offers five 16-bit timers with programmable prescaler. These timers are designated as Timer1, Timer2, Timer3, etc. The 16-bit timers can also be optionally paired to obtain 32-bit timer modules. The dsPIC30F6010 device

has eight 16-bit capture channels. The features provided by this module are useful in applications requiring Frequency (Period) and Pulse measurement. The device I2CTM module supports Multi-Master/Slave mode and 7-bit/10-bit addressing. It has two UART modules with FIFO Buffers and two CAN modules, 2.0B compliant [15].

4.2.1.4 Motor Control PWM Module Features

This module simplifies the task of generating multiple, synchronized Pulse Width Modulated (PWM) outputs. In particular, three phase AC induction motor, switched reluctance (SR) motor, brushless DC (BLDC) motor and uninterruptible power supply (UPS) applications are supported by the PWM module. This module contains four duty cycle generators, numbered 1 through 4 with 16-bit resolution. The module has eight PWM output pins, numbered PWM1H/PWM1L through PWM4H/PWM4L. The eight I/O pins are grouped into high/low numbered pairs, denoted by the suffix H or L, respectively. For complementary loads, the low PWM pins are always the complement of the corresponding high I/O pin. The PWM module allows several modes of operation which are beneficial for specific power control applications.

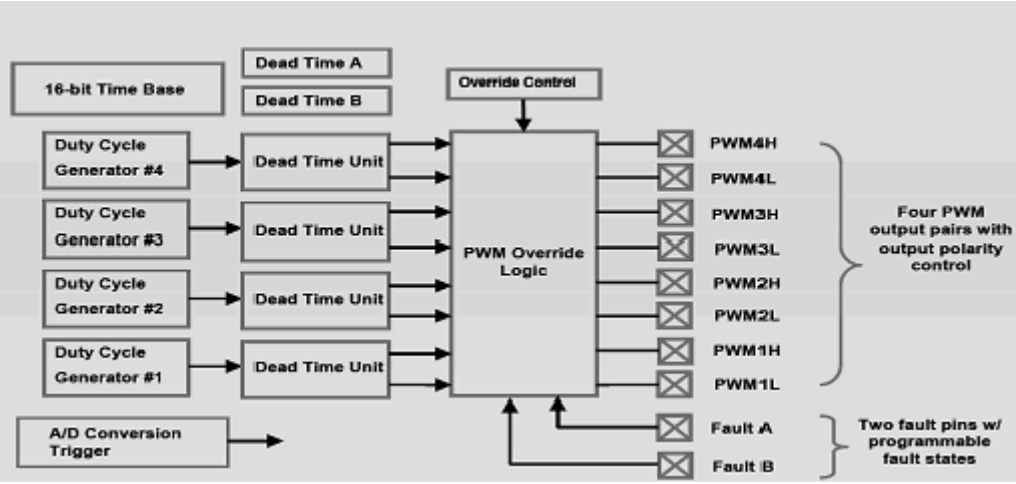

Figure 4.3: PWM module block diagram [16]

The user has the ability of changing PWM frequency ‘on-the-fly’. The PWM module can be operated in edge, center aligned output and single pulse generation modes. The module also has a feature of interrupting for asymmetrical updates in center aligned mode. The module has more advanced features such as output override control for Electrically Commutative Motor (ECM) operation, ‘Special Event’ comparator for scheduling other peripheral events, and FAULT pins to optionally drive each of the PWM output pins to a defined state [15].

4.2.1.5 Quadrature Encoder Interface Module Features

Quadrature encoders (incremental encoders or optical encoders) are used in position and speed detection of rotating motion systems. Quadrature encoders enable closed loop control of many motor control applications, such as switched reluctance (SR) motors and AC induction motors (ACIM).

A typical incremental encoder includes a slotted wheel attached to the shaft of the motor and an emitter/detector module sensing the slots in the wheel. Typically, three outputs, termed Phase A, Phase B and INDEX, provide information that can be decoded to provide information on the movement of the motor shaft including distance and direction.

The two channels, Phase A (QEA) and Phase B (QEB), have a unique relationship. If Phase A leads Phase B, then the direction of the motor is deemed positive or forward. If Phase A lags Phase B then the direction of the motor is deemed negative or reverse. A third channel, termed index pulse, occurs once per revolution and is used as a reference to establish an absolute position.

The quadrature signals produced by the encoder can have four unique states. These states are indicated for one count cycle. Note that the order of the states are reversed when the direction of travel is changed. A quadrature decoder captures the phase signals and index pulse and converts the information into a numeric count of the position pulses. Generally, the count will increment when the shaft is rotating one direction and decrement when the shaft is rotating in the other direction.

The Quadrature Encoder Interface (QEI) module provides an interface to incremental encoders. The QEI consists of quadrature decoder logic to interpret the Phase A and Phase B signals and an up/down counter to accumulate the count. Digital glitch filters on the inputs condition the input signal.

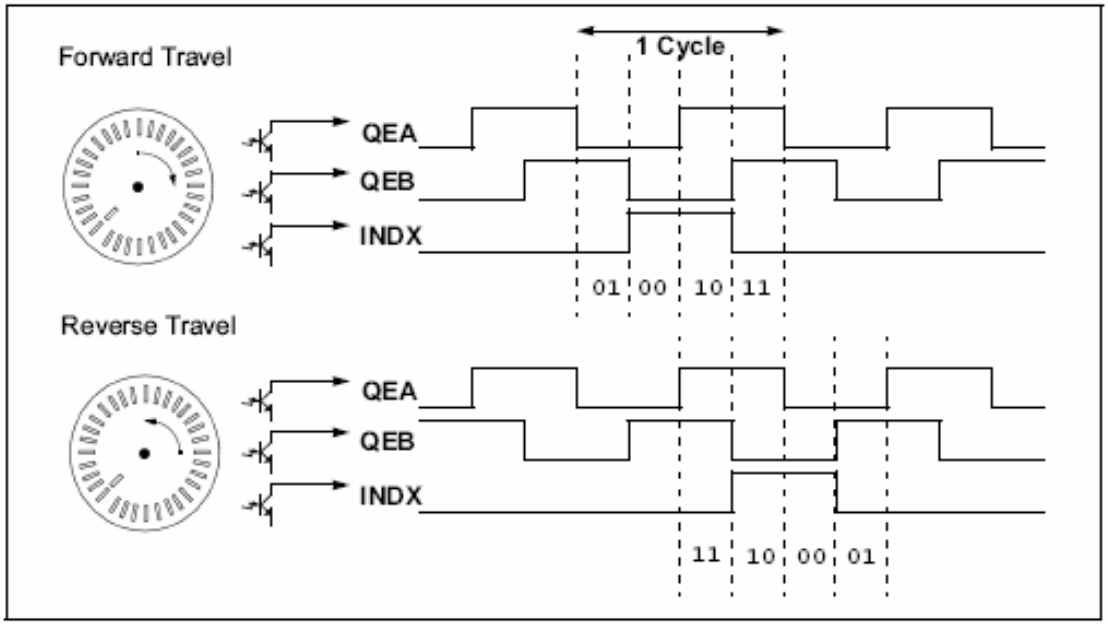

Figure 4.4: Quadrature encoder interface signals [14]

4.2.1.6 Analog Features

There is a 10-bit high-speed analog-to-digital converter (A/D) on the MC1 development board. The 10-bit high-speed analog-to-digital converter (A/D) allows conversion of an analog input signal to a 10-bit digital number. This module is based on Successive Approximation Register (SAR) architecture, and provides a maximum sampling rate of 500 ksps. The A/D module has 16 analog inputs which are multiplexed into four sample and hold amplifiers. The output of the sample and hold is the input into the converter, which generates the result. The analog reference voltages are software selectable to either the device supply voltage (AVDD/AVSS) or the voltage level on the (VREF+/VREF-) pin. The A/D converter has a unique feature of being able to operate while the device is in sleep mode.

A block diagram of the 10-bit A/D is shown in Figure 4.5. The 10-bit A/D converter can have up to 16 analog input pins, designated AN0-AN15. In addition, there are two analog input pins for external voltage reference connections. These voltage reference inputs may be shared with other analog input pins. The actual number of analog input pins and external voltage reference input configuration will depend on the specific dsPIC30F device.

The analog inputs are connected via multiplexers to four S/H amplifiers, designated CH0-CH3. One, two, or four of the S/H amplifiers may be enabled for acquiring input data. The analog input multiplexers can be switched between two sets of analog inputs during conversions. Unipolar differential conversions are possible on all channels using certain input pins (see Figure 4.5).

An Analog Input Scan mode may be enabled for the CH0 S/H amplifier. A control register specifies which analog input channels will be included in the scanning sequence.

The 10-bit A/D is connected to a 16-word result buffer. Each 10-bit result is converted to one of four 16-bit output formats when it is read from the buffer.

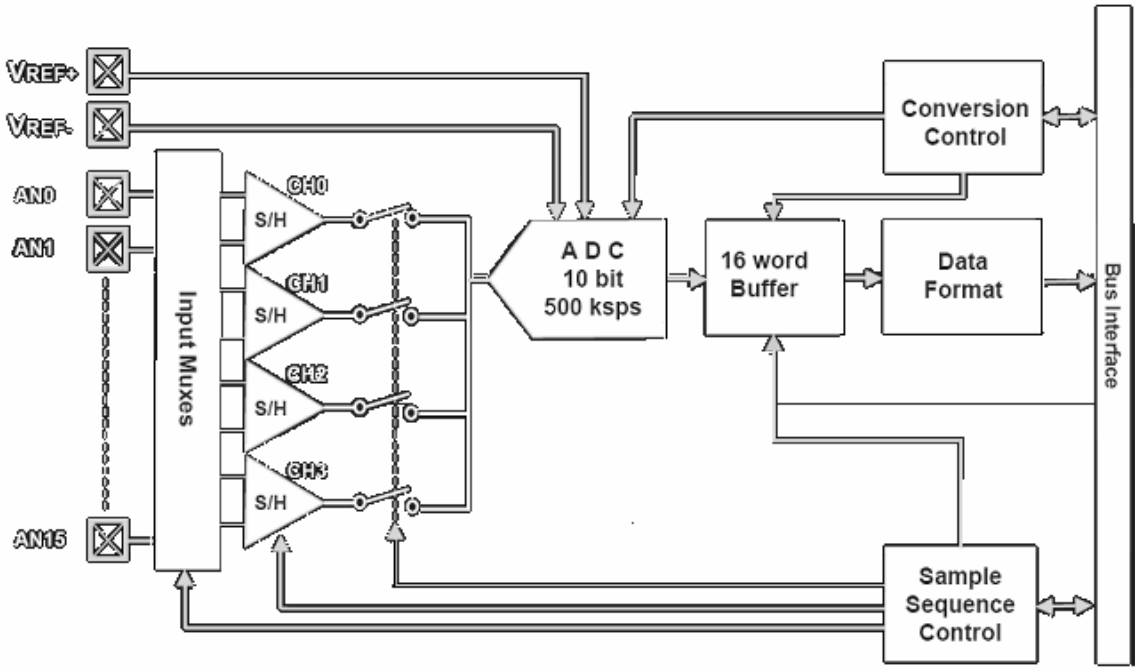

Figure 4.5: 10 bit A/D block diagram [16]

The ADCON1, ADCON2 and ADCON3 registers control the operation of the A/D module. The ADCHS register selects the input pins to be connected to the S/H amplifiers. The ADPCFG register configures the analog input pins as analog inputs or as digital I/O. The ADCSSL register selects inputs to be sequentially scanned. The module contains a 16-word dual port RAM, called ADCBUF, to buffer the A/D results. The 16 buffer locations are referred to as ADCBUF0, ADCBUF1…. ADCBUFE, ADCBUFF.

4.2.1.7 Special Microcontroller Features

These area few special microcontroller features worth mentioning:

• Enhanced Flash program memory:

- 10,000 erase/write cycle (min.) for industrial temperature range, 100K (typical).

• Data EEPROM memory:

- 100,000 erase/write cycle (min.) for industrial temperature range, 1M (typical).

• Self-reprogrammable under software control.

• Power-on Reset (POR), Power-up Timer (PWRT) and Oscillator Start-up Timer (OST).

• Flexible Watchdog Timer (WDT) with on-chip low power RC oscillator for reliable operation.

• Fail-Safe clock monitor operation detects clock failure and switches to on-chip low power RC oscillator.

• Programmable code protection.

• In-Circuit Serial Programming.

• Selectable Power Management modes.

- Sleep, Idle and Alternate Clock modes.

4.2.2 Power Supply

The main supply input to the system is via J2 (Figure 4.1). Any power supply with a 2.1 mm plug capable of delivering 9 V, up to 1 A with an unregulated AC or DC output, may be used. After rectification and filtering, the digital +5 V is created by U1 (Figure 4.1), a 1 A 2% tolerance linear regulator. The tighter than standard tolerance is used to ensure correct optoisolator drive and FAULT trip levels when using one of the

power modules. The digital +5 V is available in the prototyping area (VDD) as well as on several of the interface connectors [13].

A low current analog supply (AVDD) is created from the digital supply via a passive RC filter. This is used for the ADC in the dsPIC device and for the analog feedback signals via J1 (Figure 4.1). It is also available in the prototyping area.

4.2.3 In-Circuit Debugging and In-Circuit Serial Programming (ICSP)

In-circuit debugging and serial programming of the FLASH memory contained within the dsPIC device is supported via J4 (Figure 4.1). This allows direct connection to the MPLAB ICD 2 or the PRO MATE II via the appropriate ICSP module.

The default pins used for dsPIC emulator communication and device programming are AN1 and AN0. In order to maximize the number of ADC channels for use in motor control, provision has been made to switch the emulator and programming pins to the alternative pins of 59 and 60. These pins are shared with the low power secondary oscillator module that is not used in the design. Switching between the two sets of programming pins should be done using S2 (Figure 4.1) and the appropriate configuration bit settings within the MPLAB environment [13].

When S2 is switched to the ICD position, the analog feedback signals are disconnected from the AN0 and AN1 pins. The programming lines on J4 (Figure 4.1) are connected. When S2 is switched to the ‘Analog’ position, the programming lines are disconnected and the analog signals are connected to AN0 and AN1.

4.2.4 Motor Position Feedback Interface

Interface to two different types of commonly used motor position feedback devices is provided. Note that no electrical isolation is provided on the board. We must ensure that the motor frame is correctly earthed (grounded) and that the position feedback devices are isolated from the motor windings [13].

J3 (Halls) is intended for electrical commutation signals from (typically) Hall Effect devices. These signals are used for BLDC and SR motors and have edge transitions aligned to the electrical cycle of the motor phases. The three inputs (A, B, C) are connected to 3 input capture channels (IC1 - IC3) of the dsPIC device. Pull-up resistors and a small amount of filtering are provided on the board. The inputs are therefore, suitable for either open-collector or driven use. Clearly, the inputs can be used for any input capture or I/O requirements that we may have.

J5 (QEI) is intended for a Quadrature (or Incremental) Encoder Interface. These devices produce two position related pulse train outputs, 90° apart (A and B) and an optionally index output (Z) that pulses once per revolution. A typical device will produce many hundreds of pulses per revolution allowing high resolution position feedback and high bandwidth speed measurement. The inputs have a very small amount of filtering. Weak pull-down resistors are also fitted. The three inputs are connected through to the dedicated inputs of the QEI module of the dsPIC device.

The digital power supply (+5 V and 0 V - "G") is brought out to the connectors for powering the transducers. Series inductors are used to reduce electrical noise entering the board. The user should ensure there is adequate local decoupling of the power supply at the position transducer end of the cable. The maximum current that may be drawn from

the +5 V supply is 200 mA. If we wish to use a transducer that requires more current, then an external power supply can be used with a common connection between the grounds made on the G pin. To minimize electrical noise, a shielded cable should be used.

4.2.5 Oscillator

A 7.3728 MHz, low profile crystal (Y1) is provided on the board. In combination with the internal PLL and programmable postscaler of the dsPIC device, this allows a wide range of system clock frequencies to be generated. A low profile component is used to clear the emulator device adapter [13].

4.2.6 RS-232 Serial Port

One of the dsPIC UARTs is connected to J8 (Figure 4.1) via an RS-232 level shifting interface implemented by U5 (MAX232A). Using RG2 and RG3 as port pins also provides optional hardware handshaking using CTS and RTS. To use the handshaking, we must install links LK6 and LK7. As RG2 and RG3 are multiplexed with the I2C clock and data lines available on the digital prototyping header J7 (Figure 4.1), both features can not be used at once.

4.2.7 RS-485 Serial Bus

The second dsPIC UART is connected to J10 (Figure 4.1) via an RS-485 level shifting interface implemented by U8 (MAX485). A 120 Ω terminating resistor may be connected across the bus lines (A, B) by installing LK9. We may (optionally) control the

RX and TX enable lines by driving RG0 and RG1. Pull-down resistors are used to ensure the RX is enabled and the TX is disabled by default [13].

4.2.8 CAN bus

One of the CAN modules is connected to J9 (Figure 4.1) via a Microchip MCP2551 CAN Transceiver IC. A 120 Ω terminating resistor may be connected across the bus lines by installing LK8. A pull-down resistor ensures the TX stays inactive during RESET or if the CAN module is not being used.

The second CAN module is available on the digital prototyping header on RG0 and RG1. As these pins are used for the RS-485 RX and TX control, the RS-485 and the second CAN module may not be used at the same time.

4.2.9 LCD Display

A 16x2 LCD display (U7) is included on the board. Communication to the display is via the standard 4-bit interface method based on the well known Hitachi style communication standard.

- The LCD data lines are on RD0-RD3.
- The Enable line is on RD13.
- The Read/Write is on RC1.
- The Data/Command Select (LCDRS) is on RC3.

4.2.10 LEDs

Four general purpose LEDs (D6-D9) are provided on the board. These are connected to RA9, RA10, RA14 and RA15, respectively. A single LED (D2) is provided to indicate the +5 V supply is on. A single LED (D5) is provided to indicate direction of rotation. This is connected to RD7. When using a quadrature encoder via J5, RD7 may be automatically driven by the QEI module to indicate direction. Otherwise, this line must be driven as a port pin.

4.2.11 Push Button Switches

Four general purpose push button switches are provided (S4-S7). These are connected to RG6-RG9, respectively. A RESET switch is also provided (S1) and connected to the MCLR line of the dsPIC device.

A TRIP switch (S3) is provided which is wire ORed with an active low FAULT signal from J1 (Figure 4.1). The resulting signal (FAULT) is connected to the FLTA input of the PWM module and the OCFB input of the Output Compare module. When correctly configured in software, the TRIP switch will therefore, cause all the PWM channels to be driven to their inactive state and OC channels 5-8 to be tri-stated. Thus, the power stage may be shut down independent of software intervention. To configure the OC channels to use this feature, the OCM bits of OCxCON (x = 5-8) should all be set. To configure the PWM module to use this feature, the appropriate bits in the FLTACON register should be set.

4.2.12 Potentiometers

Two potentiometers (VR1 and VR2) are provided on the board.

VR2 is permanently connected to the AN7 input of the ADC.

VR1 is only brought to the analog prototyping header J6 as POT1 owing to analog channel constraints. If the user is not using the VPH_#1 analog feedback signal from J1, then VR2 may be easily connected to AN12 by placing a 0.1" jumper across J6. Alternatively, VR2 may be connected to any other spare analog channel by soldering a wire link between the appropriate pins of J6.

4.2.13 Prototyping Area

A 0.1" pitch prototyping area is provided on the board. Digital (VDD/VSS) and analog (AVDD/AVSS) power supplies are provided in the four corners. J6 provides access to all the ADC channels as well as having unassigned analog signals on it. J7 provides access to any optional or unassigned digital I/O pins.

CHAPTER V

DC Motor Modeling and PID Control

5.1 Introduction

DC motor speed can be controlled in different ways, some of which are by varying:

(i) flux /pole, Φ (Flux Control)

(ii) resistance R_a of the armature circuit (Rheostatic Control)

(iii) applied voltage V (Voltage Control).

These methods are not all discussed here. However, rheostatic control is discussed here since this has been used for the dynamometer project for the control of the PMDC motor. This chapter discusses the armature or rheostatic control method, next describes armature controlled DC motor modeling, and then discusses the theory of the control method adopted for the DC motor. The results for the simulations using the motor model also will be discussed in this chapter, along with experimental results.

5.2 Armature or Rheostatic Control Method

Armature or rheostatic control method is used when speeds below the no-load speed are required. As the supply voltage is normally constant, the voltage across the armature is varied by inserting a variable rheostat or resistance (called control resistance) in series with the armature circuit. As controller resistance is increased, the potential difference across the armature is decreased, thereby decreasing the armature speed. For a load of constant torque, speed is approximately proportional to the potential difference across the armature. From the speed/armature current characteristic [Fig. 5.1 (b)], it is seen that the greater the resistance in the armature circuit, the greater the decrease in speed [11].

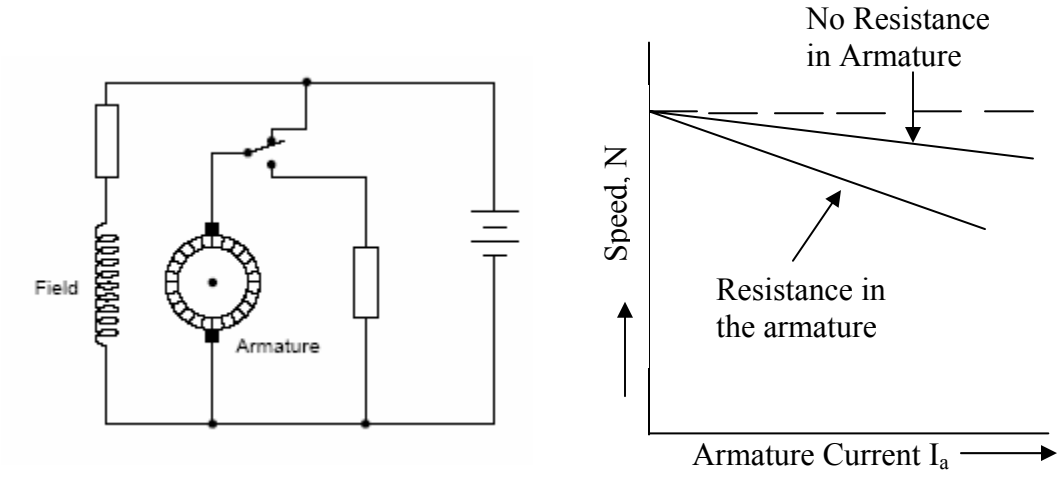

Figure 5.1 (a) Armature resistance control [11] (b) Speed/armature current characteristics.

Let, I_{a1} = armature current without armature resistance.

I_{a2} = armature current with armature resistance.

If $I_{a1} = I_{a2}$, then the load is of constant torque)

N_1, N_2 = corresponding speeds, V = supply voltage

R_a = Armature Resistance, E_{b1}= back emf without armature resistance.

Then $$N_1 \propto V - I_{a1}R_a \propto E_{b1}$$

Let some controller resistance of value R be added to the armature circuit resistance so that its value becomes $(R+R_a) = R_t$

Then $N_2 \propto V - I_{a2}R_t \propto E_{b2}$. Therefore $\frac{N_2}{N_1} = \frac{E_{b2}}{E_{b1}}$

Considering no-load speed, we have $\frac{N}{N_0} = \frac{V - I_a R_t}{V - I_{a0} R_a}$

Neglecting $I_{a0}\, R_a$ with respect to V, (since $I_{a0}\, R_a << V$) we get

$$N = N_0 \left(1 - \frac{I_a R_t}{V}\right).$$

From the above equation we see that for a given resistance R_t the speed is a linear function of armature current I_a.

The load current for which the speed would be zero is found by putting N=0 in the above relation.

$$0 = N_0 \left(1 - \frac{I_a R_t}{V}\right) \text{ or } I_a = \frac{V}{R_t}.$$

This is the maximum current and is known as the *stalling* current. This method is very expensive and unsuitable for rapidly changing loads because for a given value of R_t, speed will change with load. A more stable operation can be obtained by using a divertor across the armature in addition to armature control resistance.

5.3 PMDC Motor/Generator Mathematical Modeling

5.3.1 Modeling

Permanent-magnet motors have been widely used in high-performance electric drives and servo-systems, while permanent-magnet generators are used in the power systems. Figure 5.2 illustrates the permanent-magnet DC machine which can be used as motor and generator.

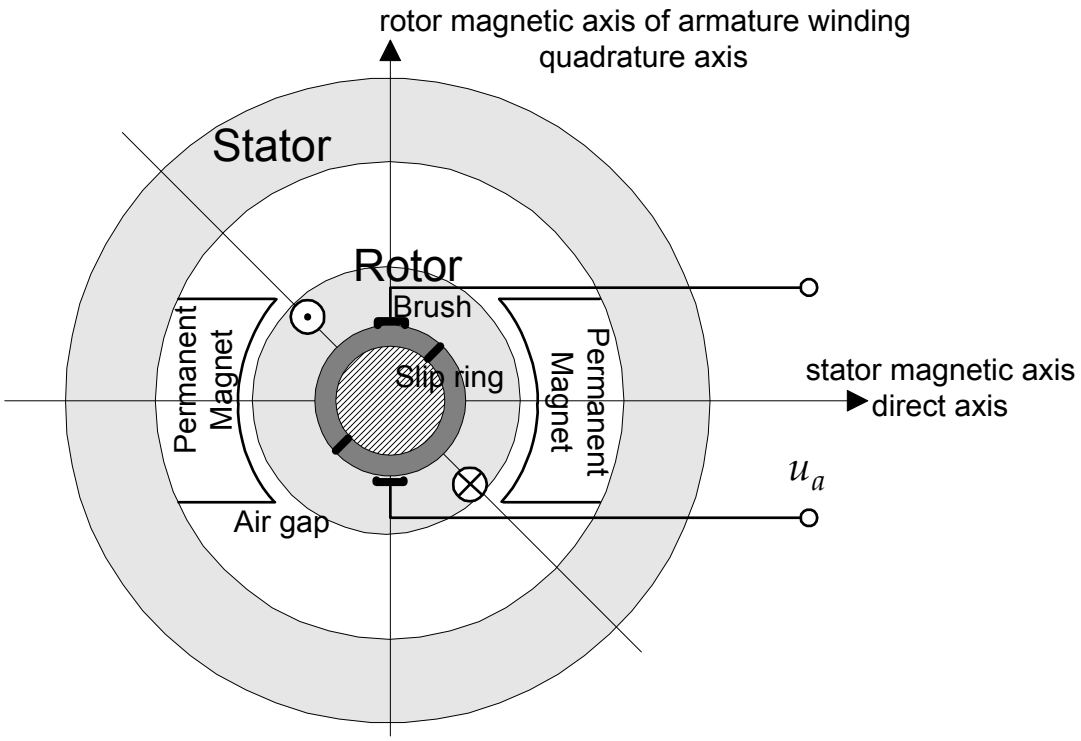

Figure 5.2 Schematic representation of a PMDC machine [17]

The permanent-magnet motors and generators are high-performance permanent-magnet electric machines, and the name plate details for the motor that was used in the project are provided in Section 2.5. We need the following parameters for the machines armature resistance r_a, armature inductance L_a, back emf or torque constant k_a, moment of inertia of the shaft J and viscous friction coefficient B_m. The angular velocity of the generator is measured using the tachometer. All the data is measured in SI units.

The mathematical model for a PMDC motor will be discussed first and then the model for the motor-generator system will be derived. The mathematical model for a PMDC is derived from both the electrical armature equations and the mechanical equations of motion [17]. A schematic diagram of a PMDC machines that is used to derive a mathematical model is illustrated in Figure 5.3.

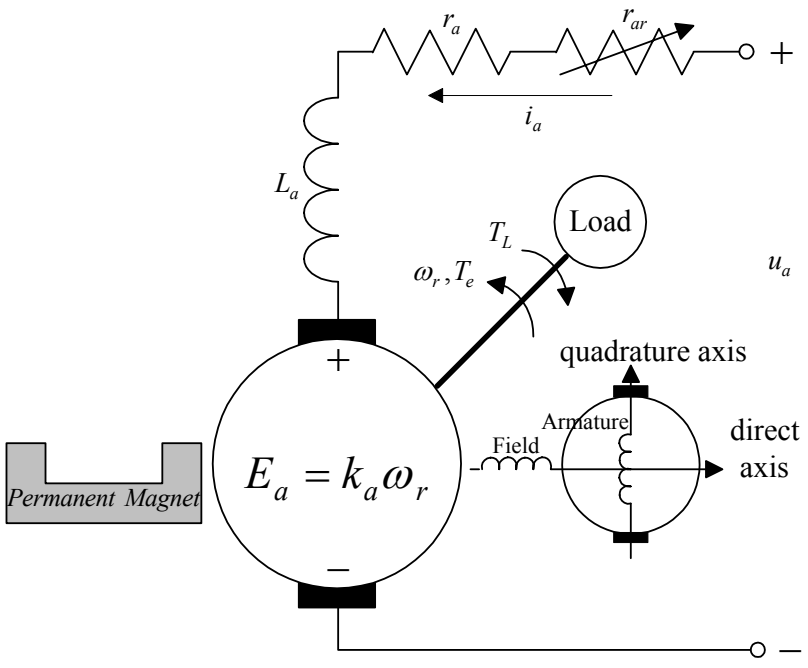

Figure 5.3 Schematic diagram of permanent-magnet electric machine (current direction corresponds to the motor operation) [17]

Using Kirchhoff's voltage law and Newton's second law of motion, the differential equations for permanent-magnet DC machines can be easily derived. Assuming that the *susceptibility* is constant (in reality, Curie's constant varies as a function of temperature), one supposes that the flux, established by the permanent magnet poles, is constant. Then, denoting the *back emf* and *torque* constants as k_a, we have the following differential equations describing the transient behavior of the armature winding and *torsion-mechanical* dynamics.

If i_a is the armature current in a PMDC motor, r_a is the armature resistance of a PMDC motor, k_a is the torque constant or back emf constant, ω_r is the speed of the rotor or shaft of the PMDC motor, u_a is the applied voltage to the motor, L_a is the armature inductance, T_L is the load torque, J is the moment of inertia of the shaft or rotor, B_m is the viscous friction coefficient, then

$$\frac{di_a}{dt} = -\frac{r_a}{L_a} i_a - \frac{k_a}{L_a} \omega_r + \frac{1}{L_a} u_a \tag{5.3.1}$$

$$\frac{d\omega_r}{dt} = \frac{k_a}{J} i_a - \frac{B_m}{J} \omega_r - \frac{1}{J} T_L \tag{5.3.2}$$

An *s*-domain block diagram of a permanent-magnet DC motor is shown in Figure 5.4

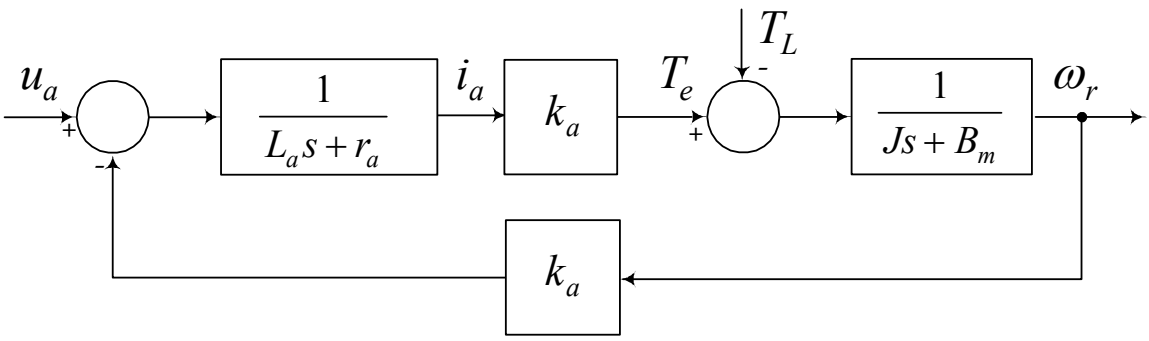

Figure 5.4 Simulink block diagram of permanent-magnet DC motor [17]

The angular velocity can be reversed if the polarity of the applied voltage is changed (the direction of the field flux cannot be changed). The steady-state torque-speed characteristic curves obey the following equation.

$$\omega_r = \frac{u_a - r_a i_a}{k_a} = \frac{u_a}{k_a} - \frac{r_a}{k_a^2} T_e \tag{5.3.3}$$

and the torque-speed characteristics are illustrated in Figure 5.5. The Figure 5.5 is the plot of steady state torque (T_e) when different voltages are applied and the plot also shows specific load torque T_L with speed.

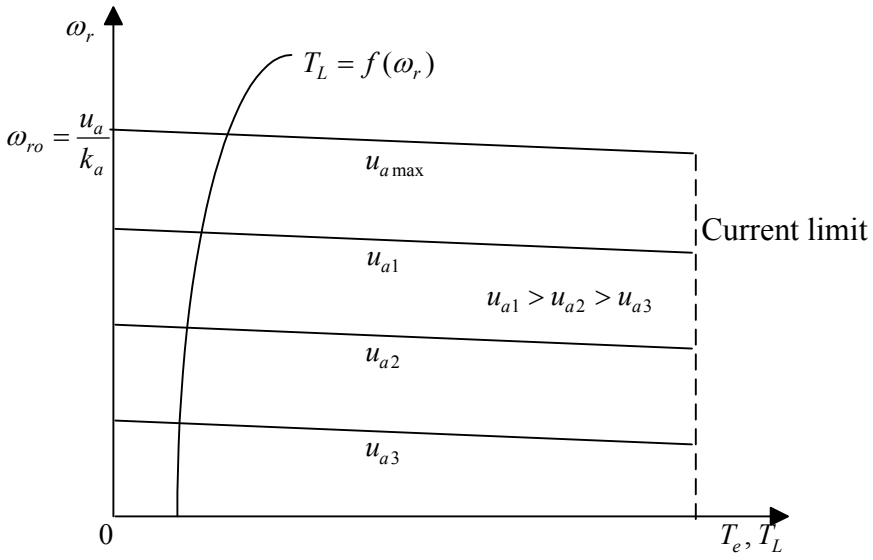

Figure 5.5 Torque-speed characteristic curves for permanent-magnet motors [17]

The steady state torque-speed curves are obtained from the specifications of the motor when they are calculated using the equations for speed and torque. A family of torque-speed characteristic curves was found applying equation 4.2.3.

In particular, plugging the different values of the armature voltage u_a in the equation $\omega_r = \frac{u_a - r_a i_a}{k_a} = \frac{u_a}{k_a} - \frac{r_a}{k_a^2} T_e$, the steady-state characteristics are found and plotted in Figure 5.6. The load characteristic is given by $T_L = f(\omega_r) = 0.05 + 0.0001\omega_r^2$.

The torque–speed and load characteristics for the dyno motor are simulated using MATLAB and are plotted for different input voltages varying from one to twenty-four in increments of four and are shown in Figure 5.6. The dotted lines are the no-load characteristics and the solid line is the load characteristic curve.

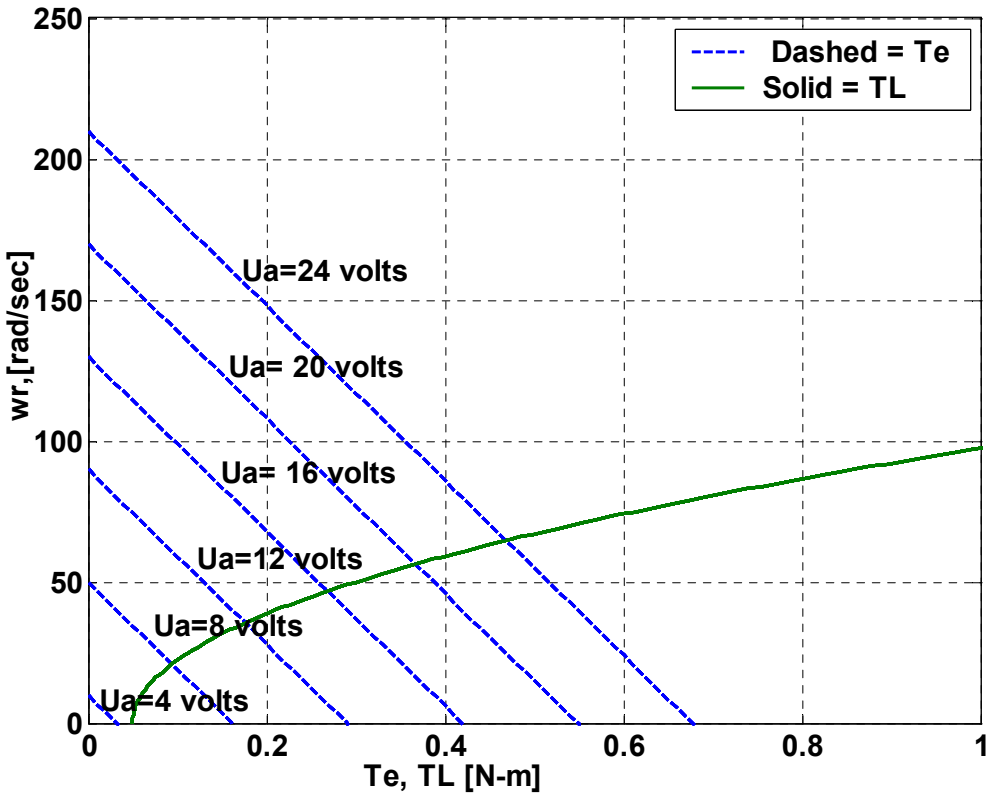

Figure 5.6 Torque-speed and load characteristic curves for DYNO Motor.

We have developed a model for a PMDC motor or generator and have seen the torque-speed and load characteristics of the dyno motor. Now the motor model needs to be simulated. We can use the simulink block diagram as shown in Figure 5.4 or use a state space model and simulate the motor using the parameters of the DC motor.

5.3.2 Simulations

As both the Simulink block diagram and the state space model are available for the dyno motor, the simulations for both the models and hence transient responses (motor behavior) for different applied voltages and load torques are done. The differential equations of the permanent-magnet DC motors were found to be,

$\frac{di_a}{dt} = -\frac{r_a}{L_a} i_a - \frac{k_a}{L_a}\omega_r + \frac{1}{L_a} u_a$, $\frac{d\omega_r}{dt} = \frac{k_a}{J} i_a - \frac{B_m}{J}\omega_r - \frac{1}{J} T_L$ (see Equations 5.3.1, 5.3.2)

Equation 5.3.1 and Equation 5.3.2 can be represented in state space form as,

$$\begin{bmatrix} \frac{di_a}{dt} \\ \frac{d\omega_r}{dt} \end{bmatrix} = \begin{bmatrix} -\frac{r_a}{L_a} & -\frac{k_a}{L_a} \\ \frac{k_a}{J} & -\frac{B_m}{J} \end{bmatrix} \begin{bmatrix} i_a \\ \omega_r \end{bmatrix} + \begin{bmatrix} \frac{1}{L_a} \\ 0 \end{bmatrix} u_a \qquad (5.3.4)$$

Denoting the state and control variables to be $x_1 = i_a$, $x_2 = \omega_r$ and $u = u_a$, the state space form can be represented as,

$$\begin{bmatrix} \frac{dx}{dt} \end{bmatrix} = \begin{bmatrix} \frac{dx_1}{dt} \\ \frac{dx_2}{dt} \end{bmatrix} = \begin{bmatrix} -\frac{r_a}{L_a} & -\frac{k_a}{L_a} \\ \frac{k_a}{J} & -\frac{B_m}{J} \end{bmatrix} \begin{bmatrix} x_1 \\ x_2 \end{bmatrix} + \begin{bmatrix} \frac{1}{L_a} \\ 0 \end{bmatrix} u \qquad (5.3.5)$$

with initial conditions $\begin{bmatrix} i_{a0} \\ \omega_{r0} \end{bmatrix} = \begin{bmatrix} x_{10} \\ x_{20} \end{bmatrix}$.

The output is the speed hence the output equation is $y = \omega_r$.

Hence, $y = \omega_r = Cx + Du = \begin{bmatrix} 0 & 1 \end{bmatrix} \begin{bmatrix} i_a \\ \omega_r \end{bmatrix} + \begin{bmatrix} 0 \end{bmatrix} u_a = \begin{bmatrix} 0 & 1 \end{bmatrix} \begin{bmatrix} x_1 \\ x_2 \end{bmatrix} + \begin{bmatrix} 0 \end{bmatrix} u$.

Using Simulink's State-Space block, the modeling can be performed. To attain flexibility, symbolic notations are used. The simulink diagram to simulate the motor dynamics is shown in Figure 5.7

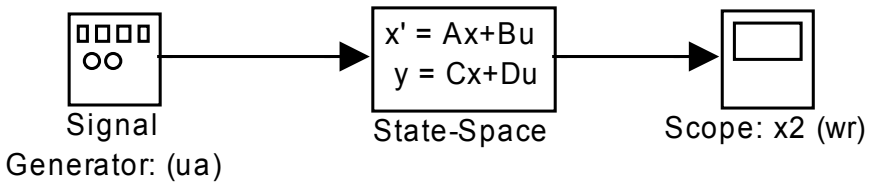

Figure 5.7 Simulink model to simulate the dyno motor.

The simulation can be performed assigning the motor parameters and initial conditions. The following motor parameters are used: r_a=3.2 ohms, L_a= 0.00535 H, k_a=0.3 V-sec/rad, k_a=0.3 N-m/A, J=0.0005 kg-m^2 and B_m=0.00001 N-m-sec/rad. The voltage is u_a=50 rect(t) V.

The initial conditions are: $\begin{bmatrix} i_{a0} \\ \omega_{r0} \end{bmatrix} = \begin{bmatrix} x_{10} \\ x_{20} \end{bmatrix} = \begin{bmatrix} 0 \\ 0 \end{bmatrix}$

To perform the simulations, in the command window we download the motor parameters and initial conditions which are mentioned above. Running the simulations and the output plot for the angular speed is as shown in Figure 5.8 below. The input voltage applied is a square wave with a period of 1 sec. As you can see from the Figure 5.8 the velocity profile follows the input voltage.

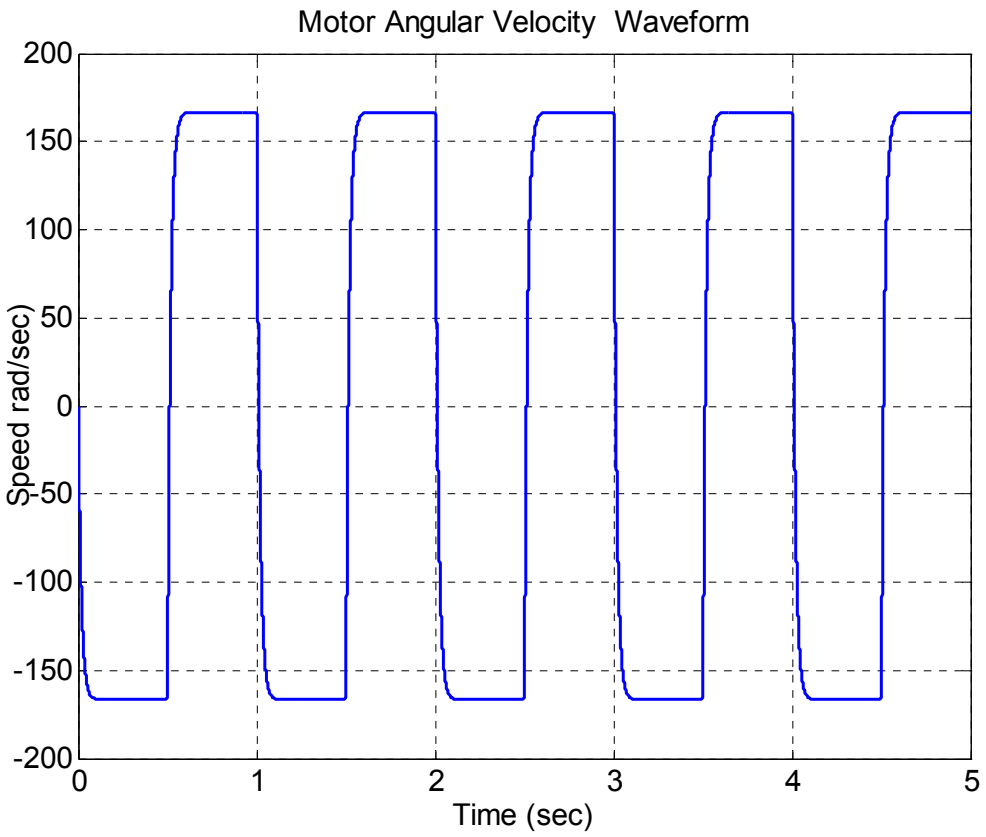

Figure 5.8 Motor angular velocity waveform.

5.4 PMDC Motor-Generator Set Mathematical Modeling

5.4.1 Modeling

The dyno system consists of a 1.25 HP DC motor (used in generator mode) fastened to an MUT (motor under test) shaft. The model for the permanent-magnet DC generator driven by the prime mover will be derived in this section and used to simulate the complete dyno model, and then the controller will be designed. The goal is to thoroughly study the transient dynamics and perform a steady-state analysis of the dyno model. To solve these problems, a mathematical model will be derived, and simulations

will be performed. Let us assume that the permanent-magnet DC motor is used as a prime mover, and the power generation system considered is illustrated in Figure 5.9 below.

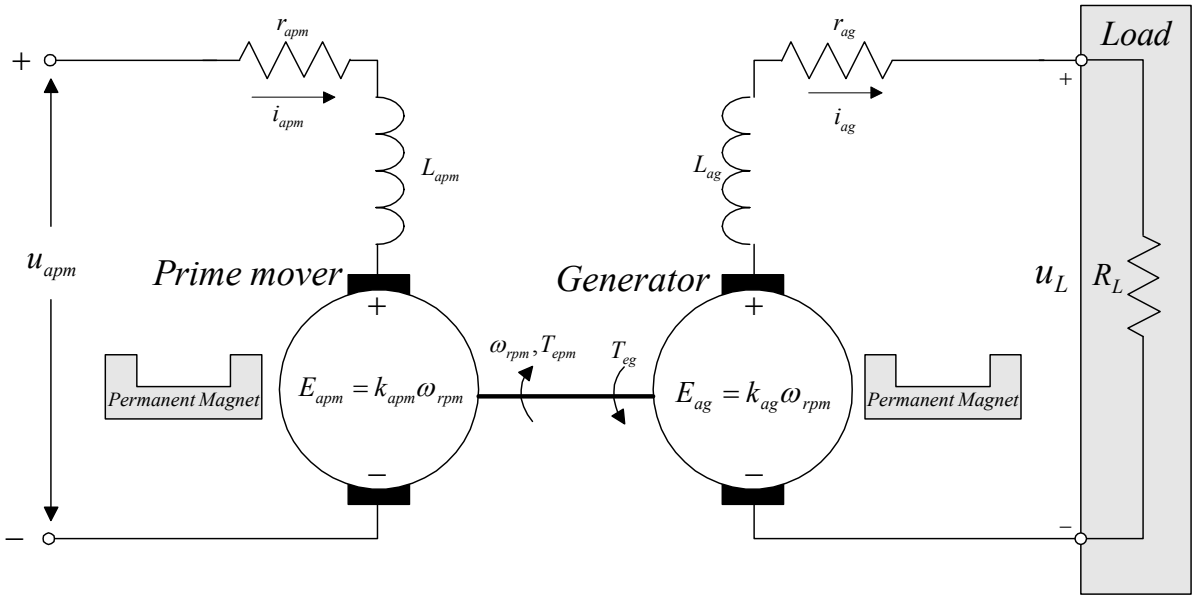

Figure 5.9 Schematic diagram of permanent-magnet DC generator driven by DC motor (MUT) [17]

The mathematical model for the permanent-magnet DC generator circuitry dynamics, if the resistive load is studied, is found using Kirchoff's law as follows [17],

$$\frac{di_{ag}}{dt} = -\frac{r_{ag} + R_L}{L_{ag}} i_{ag} + \frac{k_{ag}}{L_{ag}} \omega_{rpm} \tag{5.4.1}$$

Newton's second law of motion maps the *torsional-mechanical* dynamics of the generator–prime mover system.

$$T_{epm} - \left(B_{mpm} + B_{mg}\right)\omega_{rpm} - T_{eg} = \left(J_{pm} + J_g\right)\frac{d\omega_{rpm}}{dt} \tag{5.4.2}$$

where i_{ag} is the generator armature current; ω_{rpm} is the angular velocity of the prime mover and generator; r_{ag} and L_{ag} are the armature resistance and inductance of the

generator rotor winding; R_L is the load resistance; k_{ag} is the back emf (torque) constant of the generator; B_{mpm} and B_{mg} are the viscous friction coefficients; and J_{pm} and J_g are the moments of inertia of the prime mover and generator.

The electromagnetic torque developed by the permanent-magnet DC motor (prime mover), which is denoted as T_{epm}, is $T_{epm} = k_{apm} i_{apm}$, where i_{apm} is the armature current in the prime mover rotor winding, and k_{apm} is the back emf (torque) constant of the prime mover.

The load torque for the prime mover is the generator electromagnetic torque, and we have $T_{eg} = k_{ag} i_{ag}$.

Thus one obtains,

$$\frac{d\omega_{rpm}}{dt} = \frac{k_{apm}}{J_{pm} + J_g} i_{apm} - \frac{B_{mpm} + B_{mg}}{J_{pm} + J_g} \omega_{rpm} - \frac{k_{ag}}{J_{pm} + J_g} i_{ag} \tag{5.4.3}$$

The mathematical model for the prime mover circuitry dynamics is,

$$\frac{di_{apm}}{dt} = -\frac{r_{apm}}{L_{apm}} i_{apm} - \frac{k_{apm}}{L_{apm}} \omega_{rpm} + \frac{1}{L_{apm}} u_{apm} \tag{5.4.4}$$

where u_{apm} is the voltage applied to the armature winding of the prime mover; and r_{apm} and L_{apm} are the armature resistance and inductance of the prime mover rotor winding.

We have

$$\frac{di_{apm}}{dt} = -\frac{r_{apm}}{L_{apm}} i_{apm} - \frac{k_{apm}}{L_{apm}} \omega_{rpm} + \frac{1}{L_{apm}} u_{apm} \tag{5.4.5}$$

$$\frac{di_{ag}}{dt} = -\frac{r_{ag} + R_L}{L_{ag}} i_{ag} + \frac{k_{ag}}{L_{ag}} \omega_{rpm} \tag{5.4.6}$$

$$\frac{d\omega_{rpm}}{dt} = \frac{k_{apm}}{J_{pm} + J_g} i_{apm} - \frac{B_{mpm} + B_{mg}}{J_{pm} + J_g} \omega_{rpm} - \frac{k_{ag}}{J_{pm} + J_g} i_{ag} \,. \tag{5.4.7}$$

5.4.2 Simulations for the dyno model

In the MATLAB environment, the mathematical model derived for the permanent-magnet DC generator-DC motor generation system is used to perform simulations. In particular, a Simulink diagram is developed based upon differential equations 5.3.5, 5.3.6 and 5.3.7. Equations 5.4.5, 5.4.6 can be represented in state space form as,

$$\begin{bmatrix} \frac{di_{apm}}{dt} \\ \frac{di_{ag}}{dt} \\ \frac{d\omega_{rpm}}{dt} \end{bmatrix} = \begin{bmatrix} \frac{-r_{apm}}{L_{apm}} & 0 & \frac{-k_{apm}}{L_{apm}} \\ 0 & -\frac{r_{ag} + R_L}{L_{ag}} & \frac{k_{ag}}{L_{ag}} \\ \frac{k_{apm}}{J_{pm} + J_g} & -\frac{k_{ag}}{J_{pm} + J_g} & -\frac{B_{mpm} + B_{mg}}{J_{pm} + J_g} \end{bmatrix} \begin{bmatrix} i_{apm} \\ i_{ag} \\ \omega_{rpm} \end{bmatrix} + \begin{bmatrix} \frac{1}{L_{apm}} \\ 0 \\ 0 \end{bmatrix} u_{apm} \tag{5.4.8}$$

Denoting the state and control variables as $x_1 = i_{apm}, x_2 = i_{ag}, x_3 = \omega_r$ and $u = u_{apm}$, the state space form can be represented as,

$$\begin{bmatrix} \frac{dx_1}{dt} \\ \frac{dx_2}{dt} \\ \frac{dx_3}{dt} \end{bmatrix} = \begin{bmatrix} \frac{-r_{apm}}{L_{apm}} & 0 & \frac{-k_{apm}}{L_{apm}} \\ 0 & -\frac{r_{ag} + R_L}{L_{ag}} & \frac{k_{ag}}{L_{ag}} \\ \frac{k_{apm}}{J_{pm} + J_g} & -\frac{k_{ag}}{J_{pm} + J_g} & -\frac{B_{mpm} + B_{mg}}{J_{pm} + J_g} \end{bmatrix} \begin{bmatrix} x_1 \\ x_2 \\ x_3 \end{bmatrix} + \begin{bmatrix} \frac{1}{L_{apm}} \\ 0 \\ 0 \end{bmatrix} u \tag{5.4.9}$$

with initial conditions $\begin{bmatrix} i_{apm0} \\ i_{ag0} \\ \omega_{apm0} \end{bmatrix} = \begin{bmatrix} x_{10} \\ x_{20} \\ x_{30} \end{bmatrix}$.

The output is the speed hence the output equation is $y = \omega_r$.

Hence, $y = \omega_r = Cx + Du = \begin{bmatrix} 0 & 0 & 1 \end{bmatrix} \begin{bmatrix} i_{apm} \\ i_{ag} \\ \omega_{apm} \end{bmatrix} + \begin{bmatrix} 0 \end{bmatrix} u_a = \begin{bmatrix} 0 & 0 & 1 \end{bmatrix} \begin{bmatrix} x_1 \\ x_2 \\ x_3 \end{bmatrix} + \begin{bmatrix} 0 \end{bmatrix} u$

Therefore,

$C = \begin{bmatrix} 0 & 0 & 1 \end{bmatrix}, D = [0]$

Using the motor-generator system studied above, the transient responses and steady-state characteristics for different loads and different angular velocities of the prime mover, which depend upon the armature voltage applied u_{apm}, are examined. The induced voltage by the generator u_L and i_{ag} for different loads and angular velocity are calculated. The State-Space block in Simulink is shown in Figure 5.10.

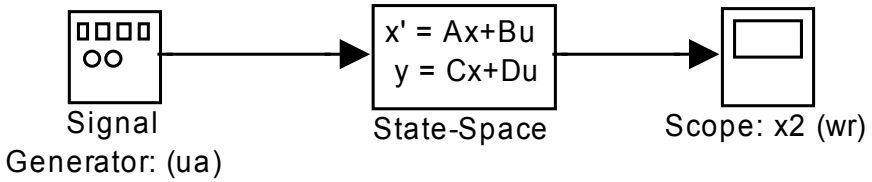

Figure 5.10 Simulink diagram to simulate the motor-generator dynamics

The transient responses for different loads (R_L) are shown in Figure 5.11 below.

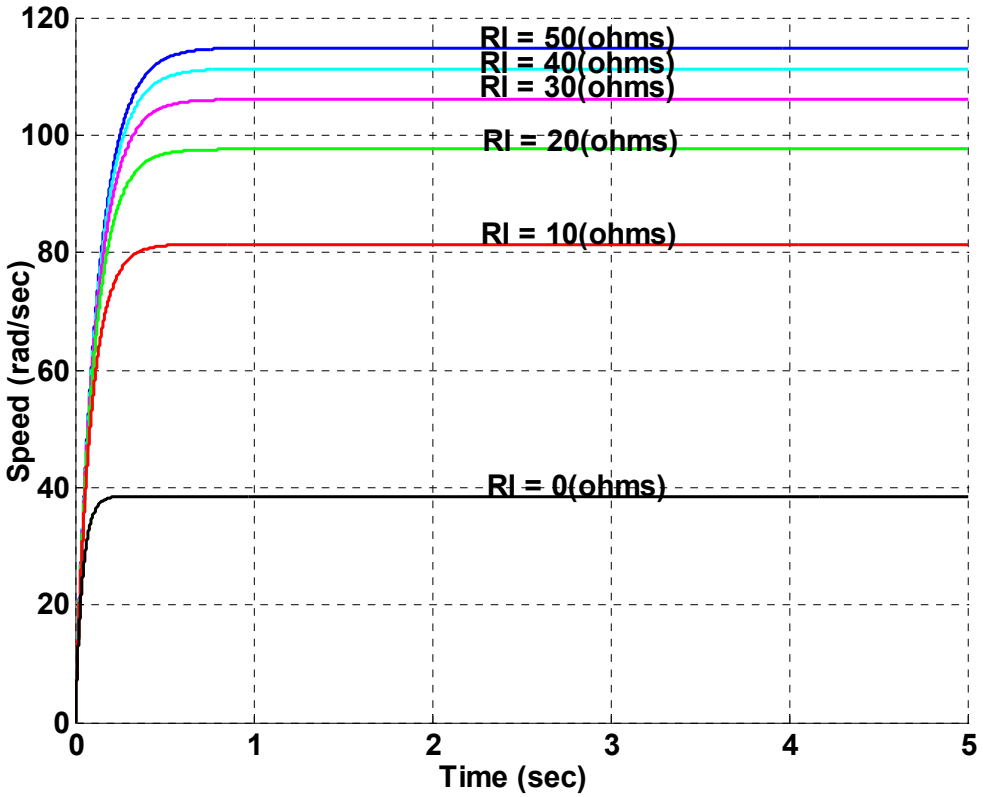

Figure 5.11 Plot of angular speeds (ω) for different loads (RL).

The steady state response of angular velocities with different loads is also shown in Figure 5.12 below.

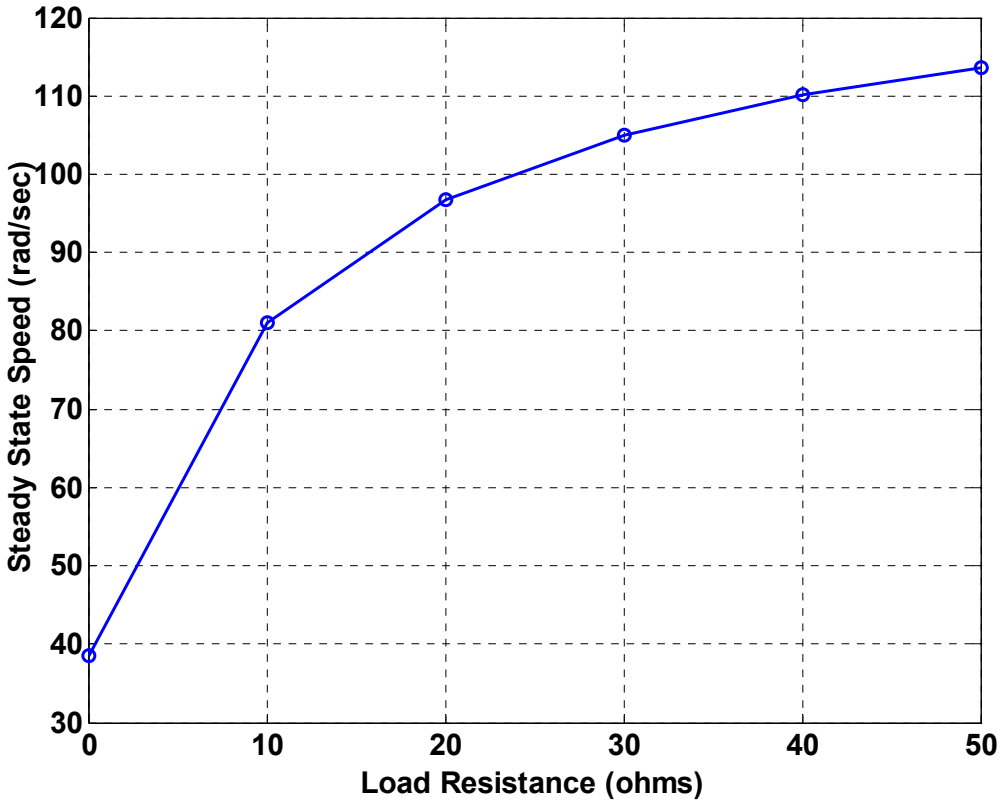

Figure 5.12 Plot of steady state angular speed (ω) for different loads (RL).

5.5 Proportional Integral Derivative (PID) Control

5.5.1 Introduction

When the control problem is to regulate the process output around a set point, it is natural to consider *error* as an input, and it follows that the integral of the error and the derivative of the error may be useful inputs as well. One such widely used form of controller to regulate the process output around a set point is the PID or three-term controller. This form of control is used extensively in industry and yet is understood, for the most part, in a way that is limited and superficial. To fully understand this type of control it is imperative that each individual component be considered separately. The

proportional component responds to present error and provides a decrease in system rise time. The integral component responds to past error by accumulating the area beneath the error curve. The integration process provides zero steady-state error with a tendency to increase overshoot and settling time. The derivative component looks at future error by responding to rate of change of error. This tends to reduce overshoot and settling time but at the same time is very susceptible to noise in the system [18].

5.5.2 PID Controller

This section will describe the characteristics of the each of proportional (P), the integral (I), and the derivative (D) controls, and how to use them to obtain a desired response. In this section, the unity feedback system of Figure 5.13 is considered.

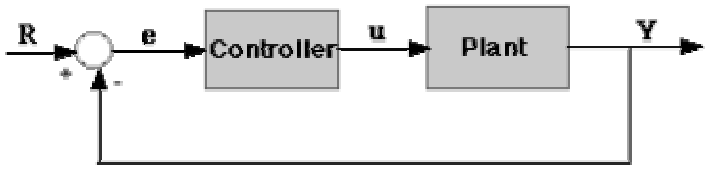

Figure 5.13 Unity feedback system [18]

In Figure 5.13 the plant is a system to be controlled, and the controller provides the excitation for the plant, designed to control the overall system behavior. The transfer function of the PID controller looks like the following:

$$K_p + \frac{K_I}{s} + K_D s = \frac{K_D s^2 + K_p s + K_I}{s}$$

where, K_p = Proportional gain, K_I = Integral gain and K_D = Derivative gain.

The variable (e) represents the tracking error, the difference between the desired input value (R) and the actual output (Y). This error signal (e) will be sent to the PID controller, and the controller computes both the derivative and the integral of this error signal. The signal (u) just past the controller is now equal to the proportional gain (K_p) times the magnitude of the error plus the integral gain (K_I) times the integral of the error plus the derivative gain (K_D) times the derivative of the error.

$$u = K_p e + K_I \int e dt + K_D \frac{de}{dt}$$

This signal (u) will be sent to the plant, and the new output (Y) will be obtained. This new output (Y) will be sent back to the sensor again to find the new error signal (e). The controller takes this new error signal and computes its derivative and it's integral again. This process goes on and on.

5.5.3 PID Characteristics

A proportional controller (K_P) will have the effect of reducing the rise time and will reduce, but never eliminate, the steady-state error. An integral control (K_I) will have the effect of eliminating the steady-state error, but it may make the transient response worse. A derivative control (K_D) will have the effect of increasing the stability of the system, reducing the overshoot, and improving the transient response. Effects of each of controllers K_P, K_D, and K_I on a closed-loop system are summarized in Table I below.

Table I PID Characteristics [18].

CL RESPONSE	RISE TIME	OVERSHOOT	SETTLING TIME	S-S ERROR
Kp	Decrease	Increase	Small Change	Decrease
K_I	Decrease	Increase	Increase	Eliminate
K_D	Small Change	Decrease	Decrease	Small Change

Note that these correlations may not be exactly accurate, because KP, KI, and KD are dependent of each other. In fact, changing one of these variables can change the effect of the other two. For this reason, the table should only be used as a reference when determining the values for K_I, K_P and K_D.

5.5.4 Simulations for the dyno system using PID controller

The dyno system consists of 1.25 HP DC motor (used in generator mode) fastened to an MUT (motor under test) shaft. The model for the permanent-magnet DC generator driven by the prime mover derived in Section 5.4 is used as a plant. The speed of the 1.25 HP DC motor is measured and the simulations were performed to track a reference speed. The simulations are done using Matlab and three different controllers are used to check the results. The controller changes the value of the load resistor (R_L) of the generator to track the reference speed. The simulation for the plant with a P controller to track a reference speed of 80 rad/sec is shown in Figure 5.14. The proportional gains used in the simulation is $K_P = 0.02$. This is the best K_P obtained when tuned for the speed to go to a steady state without much over shoot. The simulation results (Figure 5.14) has initial

overshoot because there is always a tradeoff between overshoot and the speed tracking the reference speed.

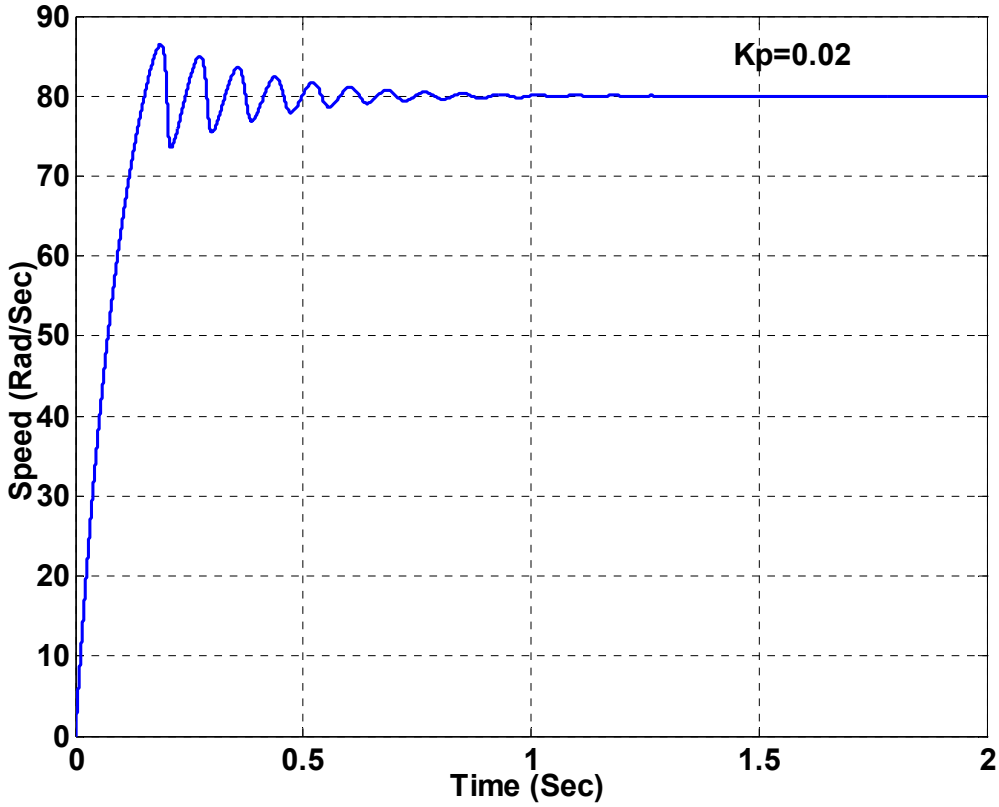

Figure 5.14 Speed plot with a P controller for a reference speed of 80 rad/sec

Figure 5.15 below shows the speed of the motor with PD control. From Figure 5.15 it can be inferred that with the PD controller applied to the plant (dyno system) overshoot decreases as compared to P controller. The number of oscillations as well as the magnitude of the oscillations decreases. With PD controller it can be observed that the settling time has decreased too. There are no oscillations of the speed of the motor after 1.5 seconds. The K_P and K_D values used in the simulations are $K_P = 0.02$ and

K_D = 0.0042. These are the best K_P and K_D obtained when tuned for the speed to go to a steady state without much overshoot and steady state error.

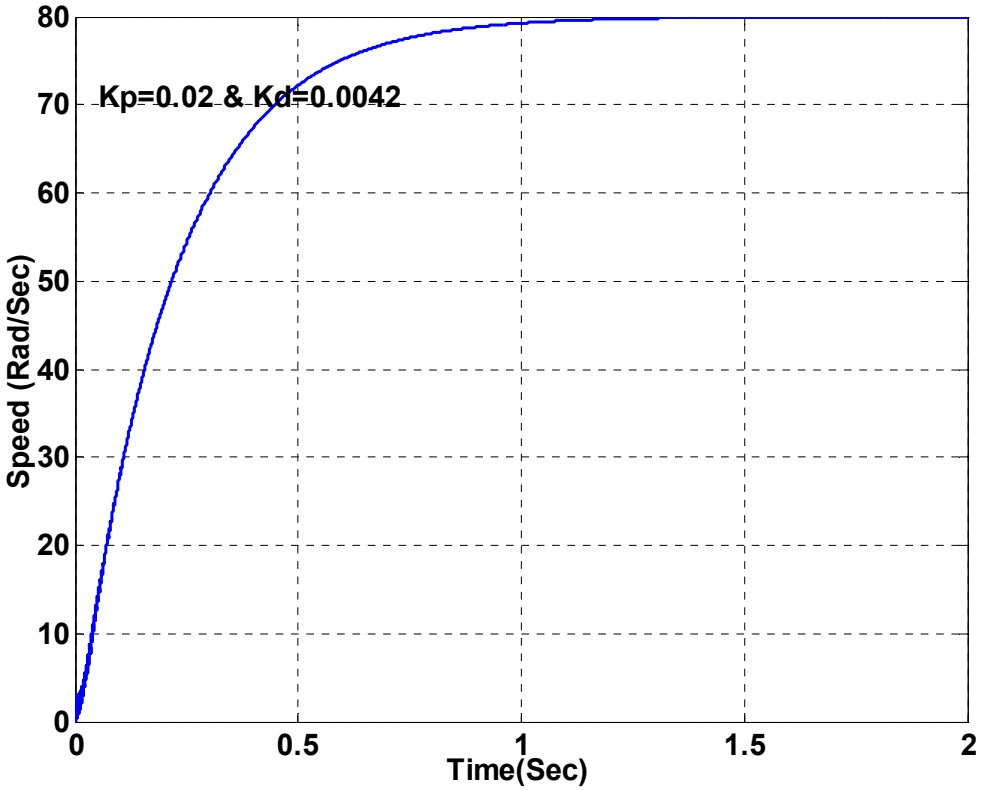

Figure 5.15 Speed plot with a PD controller for a reference speed of 80 rad/sec

Figure 5.16 shows the speed of the motor with PID control. From Figure 5.16 it can be inferred that the PID controller applied to the plant (dyno system) is the best possible controller. It can be observed that the steady state error has been removed and there are no oscillations in the system. The reference speed is reached quickly and also the response is faster compared to just a P controller. The simulations results can be basis for the experimental results. The simulations results are obtained for an initial load resistance of 40Ω. The K_P, K_D and K_I values used in the simulations are K_P = 0.2, K_D = 0.008 and K_I = 0.00472. These are the best K_P, K_D and K_I obtained when tuned for the

speed to go to a steady state faster (0.2Sec), without much overshoot and no steady state error.

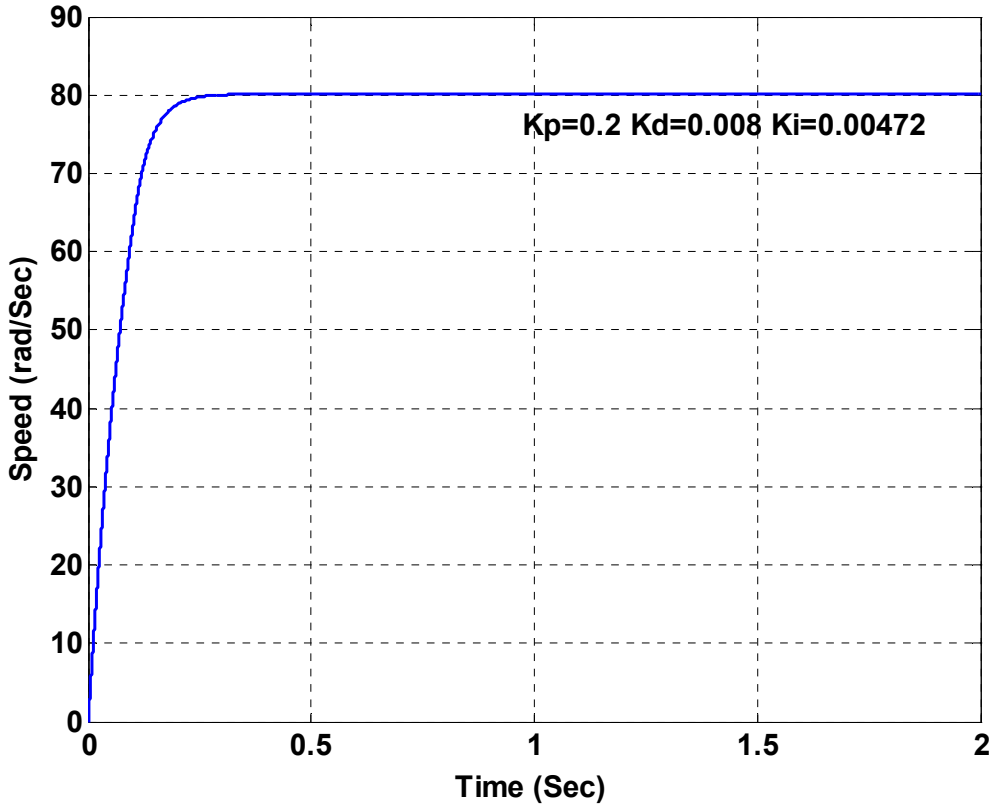

Figure 5.16 Speed plot with a PID controller for a reference speed of 80 rad/sec

5.6 Experimental Results

The experimental results are obtained by running the motor and P controller. The speed is measured using the tachometer attached to the dyno motor by the motor control development board controller using change notification on the pin technique. The user sets the reference speed using the potentiometer on the controller. Depending on the reference speed the controller (MC1 board) generates the PWM signal by varying the duty cycle in the control loop. The error speed has a proportional gain (0.5) which is

tuned for best response of the system. The no load speed of the motor is observed to be 1076 rpm. Using the potentiometer the speed is varied from 0 to 1023 rpm.

Figure 5.17 shows the waveforms obtained from the oscilloscope at motor speed of 1023 rpm. The channel 3 waveform is the tachometer (optical encoder) signal and channel 4 is the PWM signal generated from the controller. The frequency signal of the tachometer signal linearly decreases with the speed.

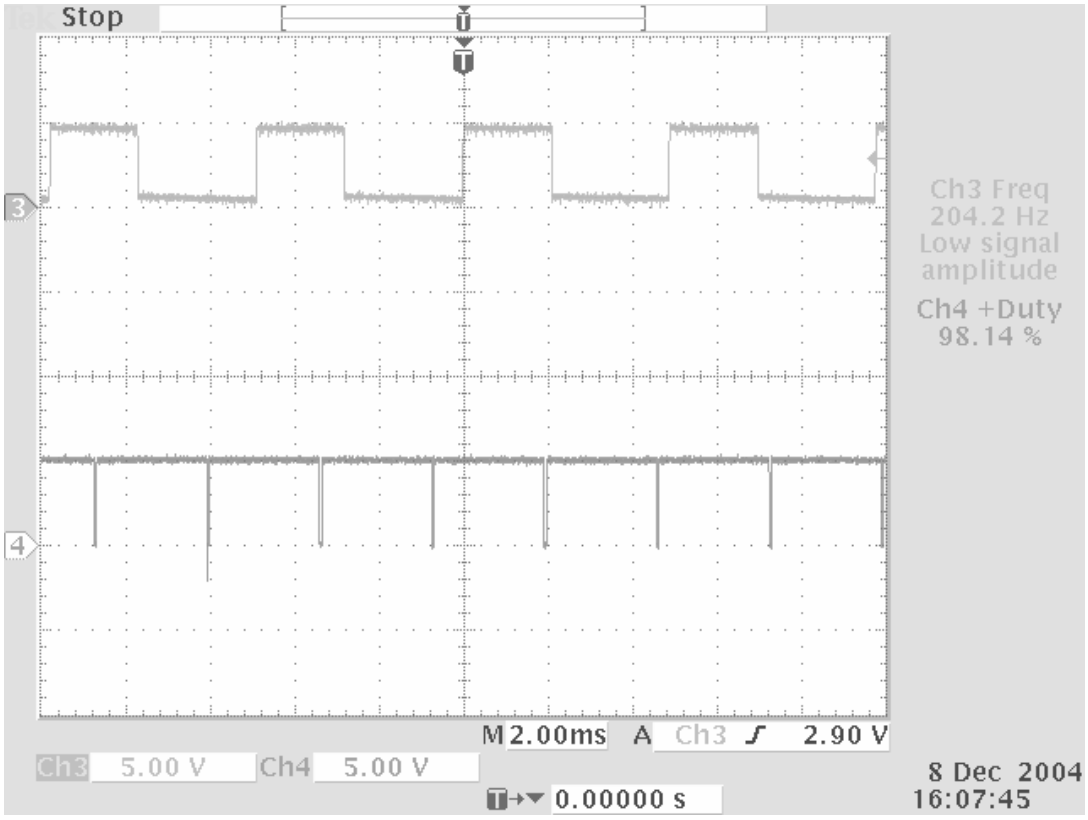

Figure 5.17 Tachometer and PWM signals for reference speed of 1023rpm

Figure 5.18 shows the watch window of the microcontroller development system, and how the speed has changed to 1023 rpm which is same as the reference speed.

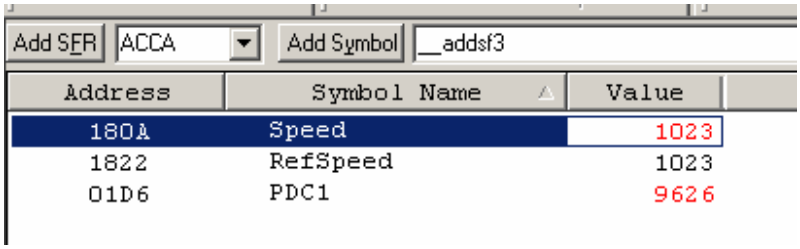

Figure 5.18 Watch window for reference speed of 1023rpm

Figure 5.19 shows the waveforms obtained from the oscilloscope at motor speed of 765 rpm. It is observed that the tachometer signal's frequency has decreased compared to the 1023 rpm signal. The duty cycle applied by the controller for a speed of 765 rpm is shown in channel 4 signal which is 92.81%.

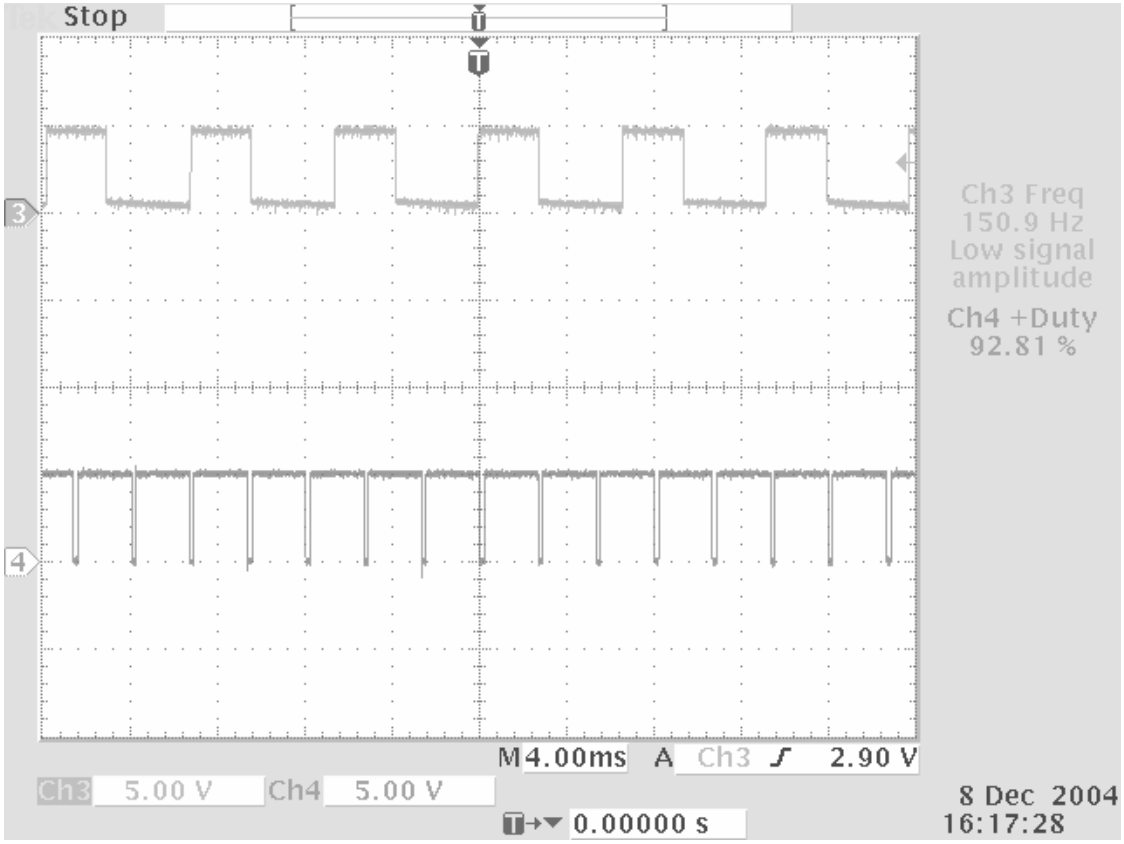

Figure 5.19 Tachometer and PWM signals for reference speed of 765rpm

Figure 5.20 shows the watch window how the speed has changed to 765 rpm which is close to the reference speed.

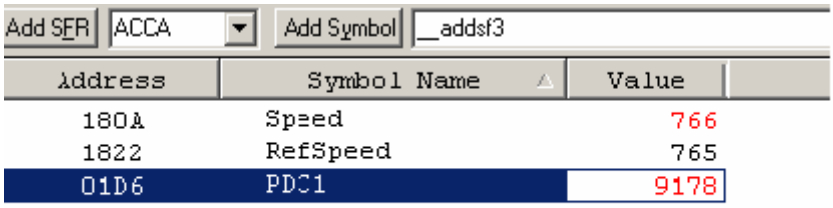

Figure 5.20 Watch window for reference speed of 765rpm

Figure 5.21 shows the waveforms obtained from the oscilloscope at motor speed of 434 rpm. It is observed that the tachometer signal's frequency has further decreased compared to the 1023 rpm signal. The duty cycle applied by the controller for a speed of 765 rpm is shown in channel 4 signal which is 75.371%.

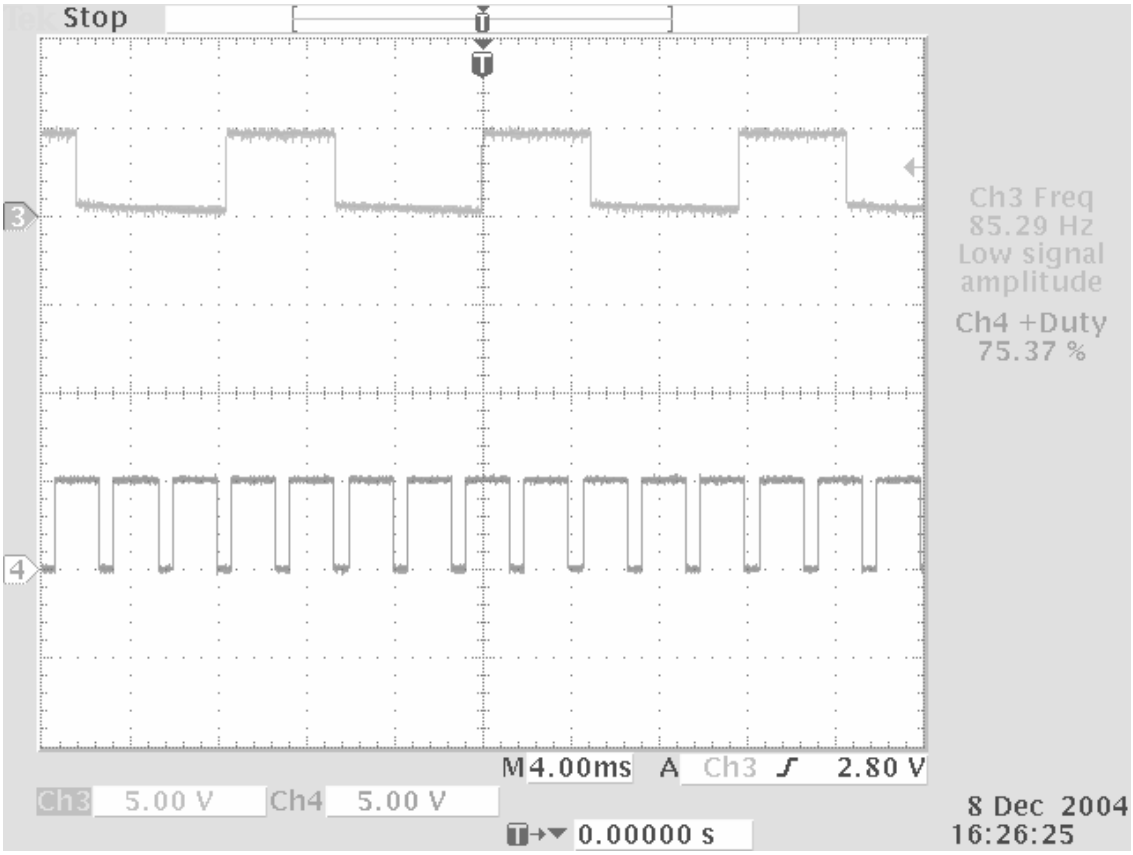

Figure 5.21 Tachometer and PWM signals for reference speed of 434rpm

Figure 5.22 shows the watch window how the speed has changed to 434 rpm which is close to the reference speed.

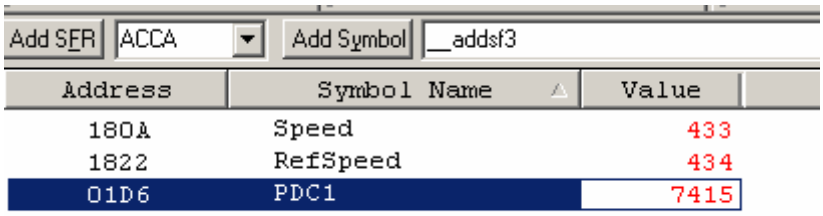

Figure 5.22 Watch window for reference speed of 434rpm

The 765 rpm speed is shown because the simulations for the model have been done for a reference speed of 80 rad/sec which is 764 rpm. The P controller simulated has a settling time of 1 sec but the settling time in real system was observed to be more than that. We need more instrumentation to more accurately observe the settling time and overshoot in the system.

CHAPTER VI

CONCLUSIONS AND FUTURE WORK

6.1 Conclusions

In this thesis a dynamometer which can be used for small power applications has been designed, tested and simulated. In industry it is hard to find a typical bench-top dynamometer, and even when one is found it may not be economically feasible for a small lab to purchase. This thesis takes dyno cost into consideration. In this thesis the traditional dynamometer with mechanical brakes has been replaced with a fully automatic digital controller. In this thesis PID control has been applied but other control techniques may also be applied to the dyno.

The mathematical model for the dynamometer has been developed which includes not just the motor model but also the PMDC generator rotated by a PMDC prime mover. The Matlab simulations for the model for different applied prime mover voltages were shown. The torque speed characteristics for the motor are also obtained and compared to the experimental results.

The simulations were performed by applying P, PD, and PID control to track a reference speed, and the results of such controls were discussed. The P control was implemented experimentally and compared to the simulation results.

6.2 Future Work

Though the automatic controller has been implemented for the dynamometer system the hardware is not fully assembled. The microcontroller and servo amplifier which were used in the originally developed dynamometer have been replaced with the MC1 motor control development board but the hardware assembly is not complete.

The control of the speed is done by dissipating heat in the load resistor by using the dyno motor in generator mode. A better method such as regenerative braking can be used, in which the DC voltage generated is converted to AC by using an inverter to supply the main power supply. The AC voltage can then be frequency controlled, and hence the speed of the motor can be controlled.

Due to time constraints only speed control has been implemented in hardware, but this work can be extended to torque control. Torque control can be done by measuring the current in the armature of the dyno motor working in generator mode.

The dynamometer 1.25 HP motor is a large motor and the shaft of the motor has high moment of inertia so the motor could be replaced with a smaller PMDC motor. The dynamometer project is an evolving project, and the final result of its development is not yet known. This thesis is an attempt to help the next developer in understanding the dyno and coming up to speed on the on-going dyno project.

REFERENCES

[1] Tom Priolo, "Baby Dynamometer Design Project," Department of Electrical & Computer Engineering, Cleveland State University, senior design project, spring 2003.

[2] Dennis Feucht, "Build Your Own Dynamometer," 1999. http://innovatia.com/Design_Center/dyno_project.htm.

[3] Magtrol, "DSP 6000 Programmable Dynamometer Controller," user's manual, July 1997, Buffalo, New York.

[4] Magtrol motor testing products description, "Dynamometers." http://www.magtrol.com/motortesting/dynamometers.htm.

[5] Magtrol, "Hysteresis Dynamometer," User's Manual, July 1997, Buffalo, New York.

[6] Magtrol motor testing products description, "Engine Dynamometers." http://www.magtrol.com/motortesting/ed_dynamometers.htm.

[7] Magtrol motor testing products description, "Dial Weight Dynamometers." http://www.magtrol.com/motortesting/dialweight_dynamometers.htm.

[8] Magtrol motor testing products description, "Eddy-Current Dynamometers." http://www.magtrol.com/motortesting/wb_dynamometers.htm

[9] Magtrol motor testing products description, "Regulator Cooler and Heat Exchanger". http://www.magtrol.com/motortesting/rer-exchanger.htm

[10] "Inside the Eddy-Current/ Powder Dynamometers." http://www.magtrol.com/motortesting/wbpb_dynamometer_inside.htm

[11] B.L.Theraja, A.K.Theraja, "A textbook of Electrical Technology in S.I units, Volume II, A.C and D.C Machines," 1998, S. Chand & Company Ltd, New Delhi.

[12] Stephen J. Chapman, "Electric Machinery Fundamentals," 1999, Third Edition, WCB McGraw-Hill.

[13] Microchip Technology Inc, Chandler, Arizona, 2003, "dsPICDEM MC1 Motor Control Development Board User's Guide" (DS70098A).

[14] Microchip Technology Inc, Chandler, Arizona, 2003, "dsPIC30F Family Reference Manual," "High Performance Digital Signal Controllers" (DS 70046B).

[15] Microchip Technology Inc, Chandler, Arizona, 2004, "dsPIC30F6010 Data Sheet" "High Performance Digital Signal Controllers" (DS70091A).

[16] Microchip Technology Inc, Chandler, Arizona, 2004, "dsPIC Digital Signal Controller (DSC) Introductory Seminar 2004" "30 MIPS Computing Power in a 6x6 mm² Package"

[17] Rochester Institute of Technology, Department of Electrical Engineering, Mechatronics Lab, Experiment # 3, "Permanent-Magnet Direct-Current Machines (Motors, Generators, and Motor-Generator System)."
www.rit.edu/~labeee/531/EE531Lab3.DOC

[18] University of Michigan, Carnegie Melon, "Control Tutorials for Matlab, PID Tutorial." http://www.engin.umich.edu/group/ctm/PID/PID.html#controller.